



Manufacturing and structural performance of glass-fiber-reinforced precast-concrete boat ramp planks

A.C. Manalo^{a,*}, O. Alajarmeh^a, D. Cooper^a, C.D. Sorbello^b, S.Z. Weerakoon^b, B. Benmokrane^c

^a Centre for Future Materials (CFM), School of Civil Engineering and Surveying, University of Southern Queensland, Toowoomba 4350, Australia

^b Boating Infrastructure Unit, Department of Transport and Main Roads, Brisbane City 4000, Australia

^c University of Sherbrooke, Department of Civil Engineering, Sherbrooke, Quebec, Canada

ARTICLE INFO

Keywords:

Boat ramp planks
Glass-fiber-reinforced polymer (GFRP) bars
Manufacturing
Time-and-motion study
Structural performance
Optimised design

ABSTRACT

Glass-fiber-reinforced-polymer (GFRP) bars are an ideal solution for eliminating the problems of steel corrosion in reinforced-concrete structures exposed to marine environments. The potential long-term benefits of the reduced maintenance costs and increased service life of GFRP-reinforced concrete structures have not been fully realized due to these reinforcing materials being more costly than steel bars. This study aims to demonstrate the cost-effectiveness of GFRP bars as internal reinforcement in precast-concrete boat-ramp planks. This is the first study that provided a comparative evaluation of the manufacturing and structural performance of planks reinforced with GFRP bars or galvanized-steel bars to fully convince engineers and asset owners of the economic benefits of specifying and using GFRP bars in infrastructure projects. The results of the study revealed that the fabrication and installation of the reinforcing mesh constituted the main differences between planks reinforced with GFRP or galvanized steel. Overall, fabricating precast-concrete boat-ramp planks with two layers of GFRP bars required less labor and equipment, and yielded better serviceability and structural performance than the current plank design using galvanized steel. These benefits led to approval and publication of the standard drawings for a new plank design for implementation in boating-infrastructure projects in Australia.

1. Introduction

In Australia, precast reinforced-concrete (RC) planks are used as platforms for recreational boat ramps [1]. Unfortunately, corrosion of the internal steel reinforcement causes the planks to deteriorate. According to the Queensland Department of Transport and Main Roads (DTMR), precast-concrete members for use in marine infrastructure should be designed based on a minimum exposure classification of A2 [2] and a minimum service life of 50 years [3]. A study conducted by Mehta et al. [4], however, concluded that the service life of RC structures in aggressive environments, such as those located in or near marine areas, is only between 20 and 30 years due to steel corrosion. Austroads [5] conducted a recent review yielding similar conclusions in that they observed that most of the concrete structures designed to have a service life of 100 years started to deteriorate only after 30 years, especially those structures built in aggressive environments. In Queensland, the economic loss associated with the expenditures for the

repair, rehabilitation, and maintenance of corrosion-damaged boating infrastructure amounts to AUD\$10 million annually [6]. Steel corrosion costs the Australian economy more than AUD\$13 billion per year [7]. Yalciner et al. [8], Mehta [9], and Cabral et al. [10] recommended different anti-corrosion design methods, including increasing the reinforcement concrete cover, installing cathodic protection, using high-performance concrete mixes, and opting for corrosion-resistant materials such as galvanized, epoxy-coated, or stainless-steel reinforcement. These methods are only temporary solutions or simply too impractical and expensive to implement and operate. Moreover, the use of these various techniques has not completely eliminated the deterioration of steel reinforcement [11]. As a result, Engineers Australia [12] has been calling for a new approach and construction technologies promising long-term solutions due to the limited resources of the state and federal governments for maintaining existing infrastructure.

The use of composite materials have been explored by many researchers to improve the cost-effectiveness of civil structures [13–15].

* Corresponding author at: Centre for Future Materials (CFM), School of Civil Engineering and Surveying, University of Southern Queensland, Toowoomba 4350, Australia.

E-mail addresses: manalo@usq.edu.au (A.C. Manalo), Omar.Alajarmeh@usq.edu.au (O. Alajarmeh), u1069746@umail.usq.edu.au (D. Cooper), Charles-Dean.A.Sorbello@tmr.qld.gov.au (C.D. Sorbello), Senarath.Z.Weerakoon@tmr.qld.gov.au (S.Z. Weerakoon), Brahim.Benmokrane@USherbrooke.ca (B. Benmokrane).

<https://doi.org/10.1016/j.istruc.2020.08.041>

Received 29 March 2020; Received in revised form 30 June 2020; Accepted 13 August 2020

2352-0124/ © 2020 Institution of Structural Engineers. Published by Elsevier Ltd. All rights reserved.

Nomenclature

α_1	Material reduction factor
α_2	Material reduction factor
β_1	Reduction factor for the compression stress block
β_{1*}	$1.1(1.6 - d/1000) \geq 0.8$
β_2	1
β_3	1
ρ_f	Reinforcement ratio
ρ_{bf}	Balanced reinforcement ratio
γ	Reduction factor for the compression stress block
ε_{cu}	Ultimate concrete compression strain (0.003)
A_{st}	Reinforcement area
b	Width of the section
c	Factor
d	Effective depth of the reinforcements
d_n	Depth of the compression concrete layer
d_v	Greater of $0.9d$ or $0.72h$
E_f	Modulus of elasticity of GFRP bars
h	Total height of the section
f'_c	Concrete compressive strength
f_{cv}	$(f'_c)^{1/3} \leq 4\text{MPa}$

f_f	Stress at GFRP bars
f_r	Modulus of rupture
f_s	Stress at steel bars
f_{sy}	Yield stress of steel bars
I_g	Moment of inertia for the gross area
k	Factor
k_m	Factor to calculate shear strength
k_r	Factor to calculate shear strength
LR	Learning rate
m	Factor
M_{cr}	Cracking moment
M_f	Factored moment force
M_u	Ultimate moment capacity
n_f	Modular ratio ($E_f/200000$)
N^m	number of work cycles
T_1	Time taken to complete the first work cycle
T_N	Time required to perform the Nth work cycle
V_f	Factored shear force
V_{uc}	Ultimate shear capacity of concrete
y_t	Half of the total plank depth

Similarly, glass-fiber-reinforced-polymer (GFRP) bars could efficiently and permanently eliminate the issue of steel corrosion in concrete structures [13–15]. Research related to this advanced construction material has been carried out extensively in the US, Canada, Europe, and Japan [16], leading to the many successful field applications of GFRP-reinforced concrete structures, including highway bridges and barriers, pavements and parking garages, storage facilities for chemical and wastewater treatment plants, revetment walls in aggressive soils, magnetic-resonance-imaging facilities, detector loops in railway lines and marine structures, and temporary structures such as soft-eyes in underground excavations and tunneling works [16]. A better understanding of the mechanical and durability properties of these materials [17–20] and of the structural behavior of GFRP-reinforced concrete structures in flexure [21,22], shear [23,24], and in compression [25–29] has increased the confidence of engineers and asset owners in using these materials. Concrete structures reinforced with GFRP bars will have significantly longer service lives, especially in marine environments [16]. Therefore, GFRP bars represent a practical replacement for the galvanized-steel internal reinforcement in planks for boating infrastructure to eliminate the issue of corrosion.

Replacing steel bars with GFRP ones in concrete slabs yielded different performances and observations. Michaluk et al. [30] and Chang and Seo [13] noticed wider, deeper, and more numerous cracks that propagated under equivalent loading conditions, reduced stiffness after initial cracking, increased bar-strain values, a tendency to fail in shear, and greater deflection at equivalent loading. These features were actually found to be controlled by different factors such as the reinforcement ratio and properties, location and number of the reinforcing layers, and concrete compressive strength [13,30–33]. Chang and Seo [13] clearly indicated that when the reinforcement ratio was increased from 0.26% to 1.20%, the maximum deflection at failure decreased by 14%, and the member stiffness after initial cracking increased. El-Sayed et al. [31], however, observed the chance of shear failure increased with increased reinforcement ratios. Furthermore, El-Nemr et al. [31] reported that using GFRP bars with a high elastic modulus of 69.3 GPa instead of 48.1 GPa but same reinforcement ratio resulted in higher cracking moments and flexural-strength capacities. The strain, cracking pattern, and deflection behavior also improved. On the other hand, Chang and Seo [13] and El-Sayed et al. [31] produced one-way slabs with double layers of GFRP bars as reinforcement and compared them to the single-layer GFRP-reinforced one-way slabs

reported on by Michaluk et al. [31]. The slabs had the same cross-sectional area, reinforcement ratio, effective depth, and clear-span length. This reduced the likeliness of premature shear failure, allowing increased load capacity and restricting crack widening, thus promoting aggregate interlocking. Lastly, Theriault and Benmokrane [34] and Ashour [32] concluded that the cracking-moment and ultimate-moment capacities increased as concrete compressive strength increased.

The potential long-term benefits of reduced maintenance costs and an increased service life for reinforced-concrete structures has been the main motivation in specifying the use of GFRP bars in a number of marine infrastructure projects. The advantageous properties and many benefits offered by using GFRP bars have not been fully realized due to the relatively higher cost of these reinforcing materials compared to conventional steel bars. Nystrom et al. [35] stated that the initial higher costs of GFRP bars made tendering processes difficult, as many contracts are awarded based on low initial costs, not on potential long-term savings. From a perspective of material costs and long-life performance, Berg et al. [36] indicated that using GFRP bars would reduce costs such as labor. Furthermore, Achillides and Pilakoutas [37] concluded that the higher initial cost of FRP materials would be offset in the long run by the reduced repair and maintenance costs of structures. Unfortunately, these observations are not well documented or quantified to fully convince engineers and asset owners of the economic benefits of specifying and using GFRP bars in infrastructure projects. Further investigation of this issue calls for adequate methods to determine the amount of resources required in manufacturing concrete structures reinforced with GFRP bars. Such information is important to critically evaluate the differences in building concrete structures with conventional steel reinforcement or GFRP bars and to demonstrate the cost-effectiveness of GFRP-reinforced concrete structures.

This study aimed at demonstrating the cost-effectiveness of GFRP bars as internal reinforcement in concrete for marine structures, going beyond simply the initial cost of materials by conducting a comparative evaluation of the fabrication and structural performance of precast-concrete boat-ramp planks reinforced with GFRP bars and planks conventionally reinforced with galvanized-steel bars. It focused on the effective design of such construction systems, conducting trial manufacturing, and performing a time-and-motion study of the manufacturing process, investigating plank structural performance, developing and validating a lean manufacturing method, and installing planks in an actual boat-ramp project. The results of this study will

provide a better understanding of the optimal design, fabrication, structural behavior, and implementation of a new construction system, thereby increasing confidence in the design and use of GFRP bars as internal reinforcement for precast-concrete elements in civil infrastructure.

2. Ramp-plank design and specifications

2.1. Design criteria

The precast-concrete boat-ramp planks were designed according to the Department of Transport and Main Road's (TMR) *Design Criteria for Boat Ramps* [1], based on the design wheel-load configuration shown in Fig. 1. The plank self-weight was approximately 2000 kg (19.62 kN). As per the provisions in AS5100.2–2017 [38], load factor of 1.2 was used for the dead load, G (Table 6.2) and a dynamic load allowance of 0.4 (Table 7.7.2, AS5100) was adopted to consider moving traffic (Q). This resulted in a design concentrated load of 36.3 kN ($1.2G + 1.4Q$) for ultimate limit strength state. In addition to this strength criteria, the precast-concrete boat-ramp planks were designed to have a 50-year design-life under exposure classification C2. AS3600-2018 [2] specifies that, in this class of exposure environment, the structural members need to have a minimum concrete compressive strength of 50 MPa and a minimum concrete cover of 65 mm over the internal reinforcement.

2.2. Design of standard GS-reinforced boat-ramp plank

The standard galvanized-steel (GS) precast-concrete plank for boat ramps (Type RG4000 planks) is designed, manufactured, and installed in accordance with the *Design Criteria for Boat Ramps* [1], MRTS72 [39], MRTS70 [40], MRTS300 [41], and AS3600-2018 [2]. The overall dimensions of the planks tested were 200 mm thick, 1000 mm wide, and 4000 mm long. These planks were reinforced in the longitudinal direction with 7 pieces of 20 mm deformed galvanized-steel bars (RBA20SG) and 28 pieces of 12 mm diameter GS bars in the transverse direction, as shown in Table 2. In addition, 4 L-shaped bent GS bars were provided to prevent concrete cracking at the corners. Fig. 2 provides the reinforcement layout. All the GS bars had a 500 MPa yield strength (grade D500N), modulus of elasticity of 200 GPa, and yield strain of 0.25% based on AS/NZS 4671 [42] (Fig. 3a). In addition, all the GS bars were ordered and delivered in the desired lengths and shapes. To achieve the required durability requirements, the GS bars were arranged in a single layer and placed at the center of the cross section of the plank, where both the longitudinal and transverse reinforcement had a clear concrete cover of at least 70 mm. A concrete compressive strength of 50 MPa with 20 mm maximum aggregate size was also used. The reinforcing bars were positioned inside the plank using a link GS bar as shown in Fig. 2b. Moreover, the DTMR requires the use of silica fume (which is expensive) to make the concrete mix watertight and to minimize corrosion of the GS bars. More details of the plank can be found in DTMR standard drawing SD4000 [43]. In this study, the GS-reinforced precast concrete boat-ramp plank was labelled SS-20–50, referring to the single layer of steel reinforcement of bars 20 mm in diameter and concrete with a compressive strength of 50 MPa.

2.3. Design of GFRP-reinforced boat-ramp planks

Two types of GFRP-reinforced precast-concrete planks were considered: one with a single layer of GFRP reinforcement (SG planks); the other reinforced with two layers of GFRP bars (DG planks). Both types of GFRP-reinforced planks were designed based on the TMR's *Design Criteria for Boat Ramps* [1], and according to CSA S806-12 [44] and the ISIS design manual [45].

2.3.1. GFRP reinforcement and concrete

Sand-coated, high-modulus vinyl-ester-based GFRP bars (Grade III) [44] were used to reinforce the precast-concrete planks (Fig. 3). The glass-fiber content by weight of the GFRP bars was around 82.1% as supplied by the manufacturer. All GFRP bars were ordered and delivered in the desired lengths. Table 1 provides the average physical and mechanical properties of the GFRP bars (standard deviation values are included between brackets), as reported by Benmokrane et al. [19]. Two nominal concrete compressive strengths were used to cast the planks, i.e., 40 MPa and 50 MPa. During concrete casting, six concrete cylinders of 100 mm in diameter and 200 mm in height were prepared from each concrete batch and tested in accordance with AS3600-2018 [2] on the same day as plank testing. The average compressive strength for the targeted 40 MPa concrete was 40.7 MPa with a standard deviation of 3.7 MPa, while the average compressive strength was 52.1 MPa for the targeted 50 MPa concrete, with a standard deviation of 2.4 MPa. It should be noted that silica fume was not used for the 40 MPa concrete since the non-corroding properties of GFRP bars precludes the need for a watertight concrete mix. The plank manufacturer [46] indicated that the silica fume increased the cost per m^3 of the concrete by 12.5%.

2.3.2. Single-layer GFRP-reinforced planks (SG planks)

The single-layer GFRP-reinforced (SG planks) had the same longitudinal and transverse reinforcement layout as SS planks (Fig. 2); the L-shaped bars were eliminated. This was possible due to the noncorroding properties of the GFRP bars, requiring a minimal concrete cover, thereby eliminating the potential for concrete cracking at the corners. The identical layout aimed at comparing the manufacturing efficiency and structural performance of the two types of RC planks, with reinforcement type being the only difference. Three single-layer GFRP-reinforced planks were prepared with two different bar sizes and two concrete strengths. Plank SG-20–40 was reinforced with a single layer of 19.1 mm GFRP bars and had a concrete compressive strength of 40 MPa. Planks SG-25–50 and SG-25–40, however, were reinforced with 25 mm diameter GFRP bars and had concrete compressive strengths of 50 MPa and 40 MPa, respectively. All the planks were reinforced in the transverse direction with 28 pieces of 12 mm diameter GFRP bars. Table 2 provides the details of these planks.

2.3.3. Double-layer GFRP-reinforced planks (DG planks)

The double-layer GFRP design (DG planks) was conceptualized potentially as an optimal design to provide the desired structural performance due to the increased effective depth of the longitudinal reinforcement. As GFRP bars are corrosion resistant, a concrete cover of 30 mm was adopted for the double-layer GFRP-reinforcement design. Two different reinforcement layouts were developed, i.e., planks reinforced with seven pieces of longitudinal GFRP bars 12.7 mm in diameter in the top and bottom layers (DG-13-40), and planks reinforced with five pieces of longitudinal GFRP bars 15.9 mm in diameter in the top and bottom layers (DG-16-40). Both these planks had very similar reinforcement ratios and were made with 40 MPa concrete. The objective of varying the longitudinal-bar diameter and the associated number of bars while keeping the reinforcement ratios relatively same was to compare manufacturing efficiency and structural performance. Another plank reinforced with seven pieces of longitudinal GFRP bars

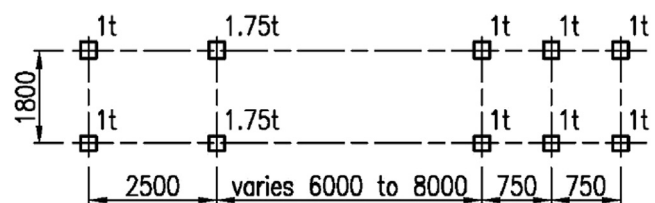


Fig. 1. Design wheel load.

Table 1
Physical and mechanical properties of the reinforcement materials [19].

Property		Test Method	Tested Sample	Value			
				No.8	No. 6	No. 5	No. 4
Physical	Nominal bar diameter, mm	CSA S806, Annex A	9	25.4	19.1	15.9	12.7
	Nominal bar area, mm ²	[44]	9	506.7	286.5	198.5	126.6
	Measured bar cross-sectional area by immersion test, mm ²			555.7	317.3	224.4	145.0
Mechanical	Ultimate tensile strength, f_u (MPa)	ASTM D7205/D7205M-06 [47]	6	1271 (29.9)	1270.0 (31.4)	1237.4 (33.3)	1281.5 (35.3)
	Modulus of elasticity, E_{GFRP} (GPa)		6	61.8 (0.3)	60.5 (0.5)	60.0 (1.3)	61.3 (0.4)
	Ultimate strain, ε_u (%)		6	2.1 (0.1)	2.1 (0.1)	2.1 (0.1)	2.1 (0.1)

Table 2
RC plank matrix and reinforcement details.

Specimen Name	Bar Type	Bar Diameter (mm)	Number of Bars	Concrete Strength, f'_c (MPa)	Reinforcement Ratio, ρ (%)
SS-20–50 (1)	GS	20	7	52.1	2.31
SS-20–50 (2)	GS	12	28	52.1	2.31
SS-20–50 (3)	GS	20	7	52.1	2.31
SG-25–50	GFRP	25.4	7	52.1	3.73
SG-25–40	GFRP	25.4	28	40.7	3.73
SG-20–40	GFRP	19.1	7	40.7	2.11
DG-13–50	GFRP	12.7	7	52.1	0.55
DG-13–40	GFRP	12.7	20	40.7	0.55
	GFRP	12.7	7		
	GFRP	12.7	18		
DG-16–40	GFRP	12.7	7	40.7	0.61
	GFRP	12.7	20		
	GFRP	12.7	18		

12.7 mm in diameter in the top and bottom layers and with a concrete compressive strength of 50 MPa (DG-13–50) was designed and fabricated to determine the effect of concrete compressive strength on the structural performance of double-layer GFRP-reinforced concrete planks. All the planks were reinforced in the transverse direction with 28 pieces of 12 mm diameter GFRP bars. Table 2 shows the longitudinal- and transverse-reinforcement details for all the tested planks. Fig. 4 shows the reinforcement details for plank DG-16–40. Steel link bars with three welded vertical plates (Fig. 4b) were fabricated to hold the bars in position. The complete details of the double-layer GFRP-reinforced concrete planks can be found in the technical drawings for Type RG4000 FRP planks [48] published by the DTMR.

3. Comparative evaluation of manufacturing performance

Past research [36,49] has indicated that the design and labor efficiencies involved with GFRP reinforcement might reduce the manufacturing requirements, potentially offsetting the higher initial purchase costs of the GFRP product. The economic benefits of specifying and using GFRP bars in infrastructure projects, however, have not been documented well enough to fully convince engineers and asset owners. This section evaluates the fabrication process of the precast-concrete planks, including a motion-and-time study for each plank type to

evaluate and compare the resources required for single and double layers of GFRP bars and single-layer GS planks. From this study, lean manufacturing methods were proposed in an attempt to streamline the process for manufacturing GFRP-reinforced planks.

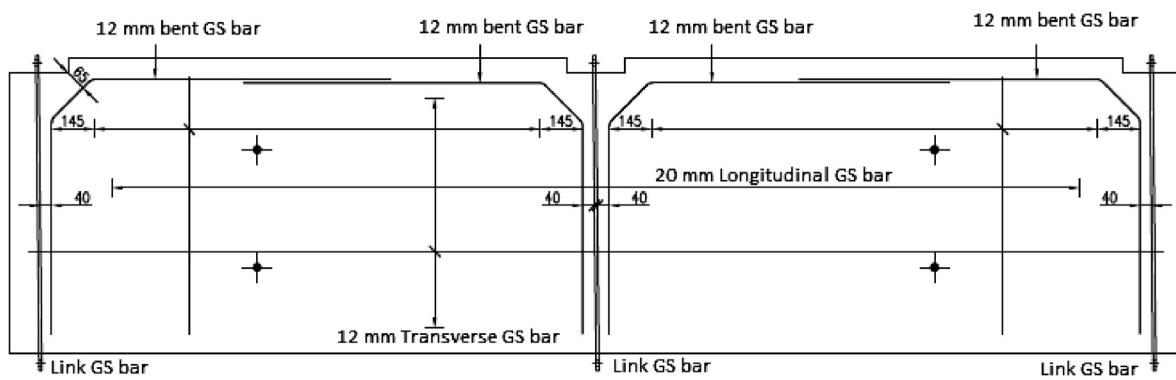
3.1. Time-and-motion study

The precast boat-ramp planks were manufactured by one of the Queensland Department of Transport and Main Roads' approved suppliers [46]. All manufacturing processes were documented and video-recorded in order to identify and analyze in detail the different processes involved, and to compare the manufacturing methods for the different types of planks. From these observations, five major processes were identified in the manufacturing of precast boat-ramp planks: (1) fabrication of the reinforcement mesh, (2) formwork setup, (3) installation of the reinforcement mesh in the formwork, (4) concrete pour, and (5) form removal. The time, labor, and equipment required to set up the formwork, concrete pour, and formwork removal was the same for all the planks. Therefore, the time-and-motion study was carried out only for the fabrication and installation of the reinforcing mesh (see Fig. 5). In the time-and-motion study, the resources required—including materials, labor, equipment, and time to complete the different individual tasks—were carefully analyzed. The information gathered was used to comparatively evaluate any cost savings involved in the fabricating precast-concrete ramp planks reinforced with GFRP bars. When necessary, a new layout and detailed design and specifications for new equipment and processes were identified and recommended.

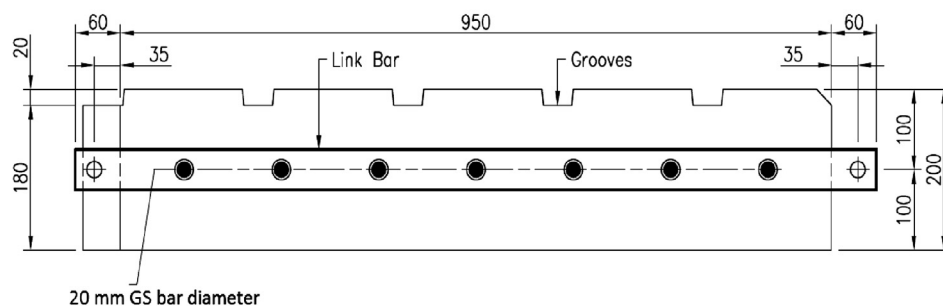
3.2. Process and activity charts

As a critical step in the motion-and-time study, process and activity charts were used to determine the differences in resources required for the mesh fabrication and installation processes for the galvanized-steel and GFRP-reinforced precast planks. This methodology was suggested by Meyers and Stewart [50] for lean manufacturing in the construction industry. In order to create the process chart, the manufacturing process was broken down into the individual tasks. The tasks were then listed in sequential order (start to finish), forming the basis of the process chart. Each task was then assigned a symbol for easy identification of the task's function. Table 3 provides the standard symbols used and their definitions. The function of each task was identified by coloring the relevant symbol adjacent to the task description (see Fig. 6). The final stage was to link each adjacent colored symbol (above and below) with an arrow. Linking symbols complete the visual flow of tasks throughout the process sequence. The overall purpose of process-chart analysis was to identify potential savings in manufacturing costs and resources by eliminating redundant tasks, combining tasks to spread costs and eliminate tasks, and changing the sequence of operations to improve product flow.

In the activity chart, the individual tasks identified in the process



(a) Layout of the longitudinal and transverse reinforcement



(b) Cross section of the plank

Fig. 2. Reinforcement details of Type RG4000 precast plank for boat ramps (SS planks).

chart were listed in sequential order; the time taken to complete each task was monitored and recorded. This made it possible to identify and analyze the tasks requiring the most time to complete. Their functions were determined by referring to the associated process chart. Subsequently, the why, what, when, where, who, and how could be examined to determine if the task time could be reduced by eliminating or reducing time-consuming tasks.

3.2.1. Mesh fabrication and installation in SS planks

Fig. 6 shows the process chart and Table 4 the activity chart for the mesh fabrication for SS planks. Based the figure and table, it took 725 s (12.09 min) to fabricate one SS-20–50 plank. Tying the steel bars together took the longest time (409.5 s), which was determined as the

average time to fabricate the three SS planks. All the tasks in the process chart were completed simultaneously by two workers who were well trained and highly competent in the fabrication process (Fig. 5a). Therefore, all tasks were completed at a standard working pace. The equipment required to complete the fabrication process includes a table to assemble the mesh, a drill to install the GS fixing ties, and a forklift to move the mesh once fabricated. Given the weight of each GS mesh (around 105 kg), five meshes were laid and fabricated on the table, and a forklift was used to carry them to the designated storage area.

During mesh installation (Fig. 5b), a total of six workers were required to complete the process: one skilled worker for driving the forklift, three workers for assisting mesh transportation and placing the mesh into the formwork, and two workers to properly place the mesh

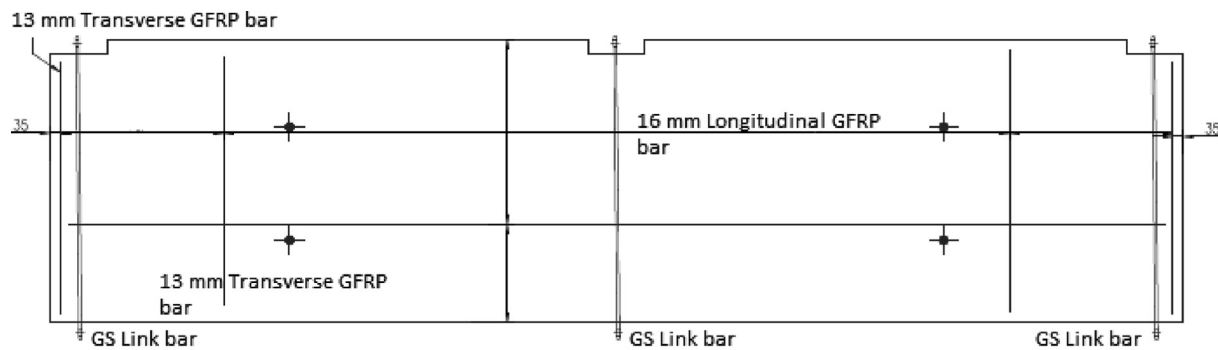


(a) Galvanized-steel (GS) bars

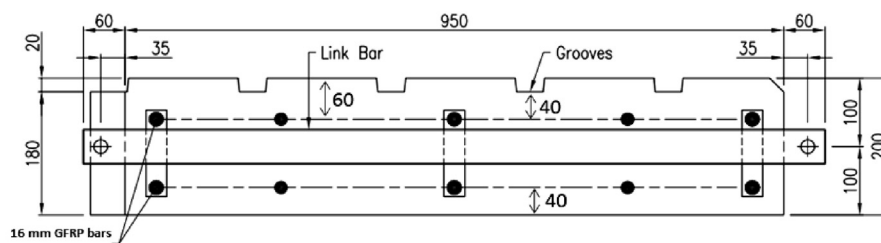


(b) GFRP bars

Fig. 3. Reinforcing materials.



(a) Longitudinal- and transverse-reinforcement layout



(b) Plank cross section

Fig. 4. Reinforcement details for Type RG4000 FRP planks.

and install the link-bar dowels connecting the planks together (see the process chart in Fig. 7 and the activity chart in Table 5). Accordingly, the time required to transfer and install the GS mesh was 58 s per mesh, with the longest time going to moving the mesh from the storage area to the formwork (around 34 s). This results in total worker time of 348 s or 5.8 min (6 workers \times 58 s) to install each GS mesh.

3.2.2. Mesh fabrication and installation in SG planks

Table 6 the activity chart for the mesh fabrication for SG planks. The fabrication of the single-layer GFRP mesh was different than that of the GS mesh due to the tool needed to tie the bars together. Instead of the drill used to fasten the ties for GS bars, a cable-tie tensioning tool was used to tie the GFRP bars together. As this fabrication method was totally new to the workers, the time needed to fabricate the single layer of GFRP mesh was 1130 s (18.82), 1124 s (18.73), and 997 s (16.62 min) for planks SG-25–50, SG-25–40, and SG-20–40, respectively. It is important to note that the reinforcement mesh for these planks was fabricated based on the order mentioned above. While the workers were not trained in using or familiar with GFRP bars, the total time for mesh fabrication clearly decreased over the fabrication cycles. As with the SS planks, all tasks during mesh fabrication for the SG planks were completed simultaneously by two workers. The equipment used was a table to assemble the mesh and a cable-tie tensioning tool (Fig. 5c). No forklift was required to lift and transport the mesh due to the light weight of the GFRP bars (around 44 kg), as shown in Fig. 5d.

Two workers installed the mesh manually. Two other workers assisted in placing the mesh in the proper position inside the formwork. Not all the workers could be considered well trained. Table 7 show that the time needed to transfer and install the GFRP reinforcing mesh was 76 s per mesh. This cannot be taken as the standard time as the workers were mastering a newly introduced installation method. The comparison of the mesh installation times revealed that GS-mesh installation was 31% faster than GFRP-mesh installation. On the other hand, six workers were needed for the GS-mesh process, while only four were required for the GFRP mesh. Taking into consideration the smaller number of workers required for GFRP-mesh installation, the total

working time to install the GFRP mesh was only 304 person-seconds or 5.07 min (4 workers \times 76 s), which is 13% faster than GS-mesh installation (348 s). It is important to note that installation of the mesh with GFRP bars did not require a forklift.

3.2.3. Mesh fabrication and installation of DG planks

The fabrication (Fig. 5e) and installation (Fig. 5f) of the reinforcing mesh for the two layers of GFRP bars (DG planks) was observed and video-recorded. The reinforcing mesh for plank DG-13–50 was the first to be fabricated, with the workers attempting to figure out the most effective fabrication method. Thus, this fabrication process was not evaluated due to the various delays in the video-recordings. For the second plank (DG-13–40), the workers required a total of 2039 s (33.98 min) to complete the fabrication process. This was cut to 1466 s (24.44 min) for the third plank (DG-16–40), as reported in Table 8. Similar to the SS and SG planks, tying the bars together took the longest time in fabricating the mesh for the DG planks. For the planks with 2 layers of GFRP bars, this task constituted 73% of the total fabrication process. Interestingly, the time required to fabricate the reinforcement mesh for the double layers of GFRP bars was twice that required to fabricate the mesh with a single layer of GS bars (2 layers \times 12.09 min).

3.3. Evaluation of the mesh fabrication and installation

It was determined that the documented manufacturing processes for the precast boat-ramp planks reinforced with galvanized-steel (SS planks) and GFRP bars (SG and DG planks) were very similar except for the mesh fabrication and installation. Table 9 summarizes the tasks, times, equipment, and labor required to complete the mesh fabrication process for the three plank types. In this table, the Total Worker Minutes was calculated by multiplying the total time for mesh fabrication and installation (in minutes) by the number of workers required. It is important to note that two workers were required for both the GS and GFRP mesh fabrication process. The comparison shows that the SS planks had the fastest mesh fabrication time, requiring only 24.18



(a) Mesh fabrication for SS planks



(b) Mesh installation in an SS plank



(c) Mesh fabrication for SG planks



(d) Mesh installation in an SG plank



(e) Mesh fabrication in DG planks








(f) Mesh installation in a DG plank

Fig. 5. Fabrication and installation of the reinforcing mesh.

worker-minutes to complete, followed by the SG planks (33.24 worker-minutes), with DG planks having the slowest fabrication time (48.88 worker-minutes). This long fabrication time was due to the process requiring a total of 32 tasks, 17 of which for transportation of materials. The longer fabrication time was also expected since the process required two mesh layers. While the fabrication of the SG planks involved fewer tasks than the SS planks (16 versus 20, respectively), the mesh

fabrication for the SG planks was 37% longer. This is likely due to workers being unfamiliar with mesh fabrication with GFRP bars. The weight of the reinforcing meshes for the SS planks (104.80 kg) required a forklift for handling, transporting, and storing. In contrast, the GFRP reinforcing mesh for the SG and DG planks were light enough to be manually carried by two workers. Regardless of the plank types or tools involved (hand drill for the SS planks and a cable-tie tensioner for the

Table 3
Process-chart symbols and definitions [50].

Symbol	Description	Indication	Definition
	Circle	Operation	Used when performing work on a part or product
	Arrow	Transportation	Used when moving materials and products
	Square	Inspect	Used for quality control
	Big D	Delay	Used for operational delays
	Triangle	Storage	Used for long-term storage

SG and DG planks), tying the reinforcement was the most time-consuming task.

The SG and DG planks had the same mesh installation time of 1.26 s per mesh, which is longer than the 0.97 min per mesh for the SS planks. The SS planks, however, required six workers and a forklift for handling and installing the reinforcing mesh, compared to four workers and no forklift for the SG and DG planks. This resulted in a total of 5.04 worker-minutes for the SG and DG planks, which was 15% faster than for the SS planks (5.82 worker-minutes). With repeated practice, combined with fewer tasks and cable-tie fastening during fabrication as well as no need for a forklift to transport the reinforcing mesh, the resources to fabricate and install the reinforcing mesh for the SG and DG planks were further reduced. This would help offset the higher initial cost of the GFRP bars compared to the GS bars. Moreover, determining the most effective use of the reinforcing material through the performance evaluation of the different planks would lead to an optimal design for which a lean-manufacturing method can be applied to increase the productivity of the GFRP-reinforced concrete planks.

3.4. Lean mesh fabrication rate

The fabrication of GFRP mesh is considered nonstandard as the process time decreased as the work cycles increased. As workers gain experience through repetition and training, the overall process becomes efficient and the time to complete tasks drops. To gain an idea of what the standard fabrication time for the GFRP mesh might be when the process has been repeated continually and workers have become practiced at the fabrication tasks, learning-curve models [51,52] were adopted and applied to predict the fabrication time for the DG planks. The univariate Crawford model [51,52] was found to be most appropriate as it provides the unit time to fabricate the N^{th} unit. This model needs the time required to complete the first work cycle in order to establish a learning rate. Afterwards, the Crawford model was used to predict the time to perform the N^{th} work cycle (see Eqs. (2) and (3)). In these equations, T_N is the time required to perform the N^{th} work cycle, whereas, T_1 is the time taken to complete the first work cycle. On the other hand, N^m is the number of work cycles in the repetitive sequence to the power of the m factor, which is the natural logarithm of the learning rate divided by the natural logarithm of 2.

$$T_N = T_1 N^m \quad (2)$$

$$m = \frac{\ln(LR)}{\ln(2)} \quad (3)$$

Groover [51,52] stated that typical learning rates (LR) can be used in the Crawford model for various types of work and industry. According to his classification (type of work and industry category), the

most relevant type of work and industry category for the RC plank fabrication is either construction or machine shop-repetitive with a corresponding LR of (70–90)% and (90–95)%, respectively. In contrast, the LR value of the fabrication was 86.8% as it is the ratio of the times required for trial 2 (16.57 min) and trial 1 (19.09 min). Assuming a conservative value, the adopted LR of 90%, which is the mutual learning rate between the two categories, was deemed suitable for the fabrication of GFRP-reinforced planks. It is to be noted however that this analysis is based on the fastest time recorded in this study. Fig. 8 shows the effect of more work cycles (N) (worker experience) on reducing the total fabrication time (T_N). Targeting the same time required to fabricate the GS mesh (12.09 min), 9 and 20 work cycles would be required to achieve the target T_N with LR of 86.8% and 90%, respectively, are used. Clearly, the mesh fabrication time for the DG planks is equal to or shorter than for the standard single-layer mesh using galvanized steel within 20 work cycles. This, combined with the 13% shorter time for placing the GFRP mesh into the formwork and the savings from not needing a forklift, leads to the conclusion that the DG plank is a structurally efficient and cost-competitive system for precast-concrete boat-ramp planks.

4. Structural performance and serviceability analysis

This section presents the evaluation of the structural performance of precast-concrete ramp planks reinforced with GFRP bars and a comparison with GS-reinforced planks. The failure mode, crack pattern and propagation, load-deflection response, mid-span deflection, flexural strength, and strains in concrete and reinforcement were measured and analyzed systematically. This will provide essential information in determining the optimal reinforcement design for precast GFRP-reinforced concrete boat-ramp planks.

4.1. Test setup and instrumentation

The planks were tested in bending in accordance with the design wheel-load configuration in Fig. 1. During plank manufacturing and prior to the tests, uniaxial electronic resistance strain gauges were attached at critical locations on the concrete surface and internal reinforcement, as shown in Fig. 9. Unfortunately, some of the strain gauges did not register any readings as they were damaged during plank demolding and transportation. The planks were simply supported with a clear-span length of 3800 mm and the loads were applied 1800 mm apart with a spreader I-beam, as shown in Fig. 10. The load was applied in displacement-control mode and measured with the 2000 kN capacity load cell. The cracking propagation was marked on the plank surface up to an applied load of 100 kN. The mid-span deflection was measured with a laser displacement sensor positioned under the center of the planks. In addition, a crack-width measuring device was attached to the plank after the appearance of the first crack to measure its width development. The applied load, strains, deflection, and crack width were recorded up until failure using a System 5000 data logger.

4.2. Cracking moment

The concrete surfaces were free of cracks prior to load application. The load at which the first crack was observed was taken as the cracking load (P_{cr}) and used to calculate the experimental cracking moment (M_{cr}). It should be noted that the M_{cr} values are also calculated including the self-weight of the plank. Therefore, the additional moment force because of the self-weight is 9.03 kN.m, calculated using Eq. A-3. Table 10 presents the values of P_{cr} and M_{cr} for all the planks tested. As shown in the table, the DG planks exhibited the highest cracking moment—at least 20.8 kN-m—which is at least 10% higher than the SS planks. This could be attributed to the increased effective depth of the flexural bars, which increased the dowel action of the longitudinal

Task	Operate	Transport	Inspect	Delay	Storage	Description
1	○	➡	□	⬢	▽	Retrieve longitudinal reinforcement (7x bars)
2	●	➡	□	⬢	▽	Spread out longitudinal bars
3	○	➡	□	●	▽	Retrieve link bar (1x bar)
4	●	➡	□	⬢	▽	Install link bar at end of longitudinal bars
5	○	➡	□	⬢	▽	Walk to opposite end of longitudinal bars
6	○	➡	□	●	▽	Retrieve link bar (1x bar)
7	●	➡	□	⬢	▽	Install link bar at end of longitudinal bars
8	○	➡	□	●	▽	Retrieve link bar (1x bar)
9	●	➡	□	⬢	▽	Install link bar at end of longitudinal bars
10	●	➡	□	⬢	▽	Move 1x link bar to centre of mesh
11	○	➡	□	⬢	▽	Retrieve transverse bars (24x bars)
12	●	➡	□	⬢	▽	Spread out transverse bars
13	○	➡	□	⬢	▽	Retrieve steel fixing device and ties
14	●	➡	□	⬢	▽	Tie steel bars (88x ties)
15	○	➡	□	⬢	▽	Retrieve additional steel fixing ties
16	○	➡	□	⬢	▽	Retrieve bent steel (4x bars)
17	●	➡	□	⬢	▽	Align bent steel onto mesh
18	●	➡	□	⬢	▽	Fix bent steel (16x ties)
19	○	➡	□	⬢	▽	Retrieve additional steel fixing ties
20	●	➡	□	⬢	▽	Place timber chocks on top of finished mesh (3x chocks)

Fig. 6. Process chart for fabricating the mesh for an SS plank.

reinforcement and aggregate interlock area in the concrete section above the longitudinal reinforcement. This was due to the bottom bars acting as links for better continuity within the concrete section. The experimental values were then compared to the theoretical value calculated with Eq. A-1), as suggested in CSA-12 [44] and ISIS Canada [45]. In this calculation, the rupture modulus of concrete (f_r) is estimated based on the concrete compressive strength (f_c') and the section geometry [Eq. A-2a]. In addition, the theoretical evaluation of the cracking moment using the suggested relation for f_r (see Eq. A-2b) in CSA-14 [53] was conducted. The results show that using f_r as reported in Eq. A-2(a) overestimated $M_{cr,1}$ if it is compared directly to the experimental results, which is similar to the findings of El-Nemr et al. [54]. However, $M_{cr,1}$ shows very good agreement with the experimental M_{cr} when the bending moment induced by the self-weight is included. While using f_r , as suggested in CSA-14 [53], underestimated the

cracking moment for the tested planks. However, the underestimation is significant for the double-layer GFRP-reinforced planks. This could be due to the high effective depth of the reinforcement increasing the shear span-to-depth (a/d) ratio, leading to the arch-action effect. It also increased the area of concrete in compression, making the plank highly resistant before cracking, as reported by El-Sayed et al. [31] and Maranan et al. [23].

4.3. Crack pattern and failure mode

After the first crack, hairline cracks developed and propagated along the length of the planks as the applied load increased. Fig. 11 shows the crack pattern and the final failure of the concrete planks. The red lines represent the cracks that developed before the service load, considered as a 30% of the ultimate applied moment, as reported in Table 11. The

Table 4

Activity chart for fabricating the mesh for an SS plank.

Task	Activity	Time (seconds)
1	Retrieve longitudinal reinforcement (7 bars)	27.14
2	Spread out longitudinal bars	9.92
3	Retrieve link bar (1 bar)	7.78
4	Install link bar at end of longitudinal bars	9.78
5	Walk to opposite end of longitudinal bars	3.92
6	Retrieve link bar (1 bar)	3.62
7	Install link bar at end of longitudinal bars	12.71
8	Retrieve link bar (1 bar)	3.85
9	Install link bar at end of longitudinal bars	3.92
10	Move 1 link bar to center of mesh	7.86
11	Retrieve transverse bars (24 bars)	18.31
12	Spread out transverse bars	17.63
13	Retrieve steel fastening device and ties	25.57
14	Tie steel bars (88 ties)	409.49
15	Retrieve additional steel fixing ties	12.17
16	Retrieve bent steel (4 bars)	21.37
17	Align bent steel onto mesh	10.94
18	Fix bent steel (16 ties)	89.36
19	Retrieve additional steel fixing ties	12.32
20	Place timber chocks on top of finished mesh (3 chocks)	17.74
Total Time (seconds)		725.41
Total Time (minutes)		12.09

thin black lines represent the cracks after the service load, and the very thick black lines represent the location of the final failure. In general, the propagation of cracks in the planks can be described as follows:

- *SS planks*: Most of the cracks developed and propagated between the loading points, as shown in Fig. 11a to c. All the planks exhibited only a few narrow cracks at service load. At advanced loading,

planks SS-20–50 (1) and SS-20–50 (2) failed by concrete compressive crushing at the mid-span length, as shown in Fig. 11a and b. Plank SS-20–50 (3), however, experienced tension–shear failure, since the adopted loading configuration can cause this type of failure [55]. Moreover, the planks had a high shear span-to-depth ratio (a/d) ratio (10), which significantly increases the probability of tension–shear failure due to greater deflection, as also reported by Kim and Park [56].

- *SG planks*: Most of the cracks developed and propagated between the loading points, with more cracks than the SS planks once the service load had been reached (see Fig. 11d to f). This may be due to the GFRP bars having higher deflection and a lower modulus of elasticity than the galvanized-steel bars [57]. The high deflection also resulted in the development of horizontal shear cracks at the level of longitudinal reinforcements at advanced loading. The final failure was tension–shear failure regardless of the reinforcement ratio and concrete compressive strength. This was due to the shallow compression zone in the concrete because of the low modulus of elasticity of the GFRP bars. Michaluk et al. [30] and Chang and Seo [13] had similar findings.

- *DG planks*: The cracks were well distributed along the plank length due to the reinforcement having greater effective depth. In addition, the cracks were narrower than in the SS and SG planks due to the tensile GFRP bars closer to the bottom concrete surface resisting the opening of the flexural cracks. The reinforcement's greater effective depth also yielded a a/d ratio lower 37.5% than that of the SS and SG planks [Table 11]. As a result, the failure of planks DG-13–40 and DG-16–40 was governed by compression–shear failure due to increased arch effect (Fig. 11h and i, respectively). Plank DG-13–50, however, experienced tension–shear failure (Fig. 11g), due to the higher concrete compressive strength compared to the other two DG

Task	Operate	Transport	Inspect	Delay	Storage	Description
1	○	➡	□	⏸	▽	Move 10x mesh to temporary position
2	○	➡	□	⏸	▽	Return to main mesh stack
3	○	➡	□	⏸	▽	Move 10x mesh to temporary position
4	○	➡	□	⏸	▽	Return to main mesh stack
5	○	➡	□	⏸	▽	Move 10x mesh to temporary position
6	○	➡	□	⏸	▽	Move to designated area to change forklift lifting device
7	●	➡	□	⏸	▽	Change forklift lifting device
8	○	➡	□	⏸	▽	Move back to closest temporary mesh stack
9	●	➡	□	⏸	▽	Pickup mesh from stack
10	○	➡	□	⏸	▽	Move to formwork
11	●	➡	□	⏸	▽	Load mesh into formwork
12	○	➡	□	⏸	▽	Return to mesh stack

Note that repeating steps 10, 11, and 12 are repeated 30 times.

Fig. 7. Process chart for installing the mesh for an SS plank.

Table 5
Activity chart for installing the mesh for an SS plank.

Task	Activity	Time (seconds)
1	Move 10 meshes to temporary position	68.81
2	Return to main mesh stack	65.08
3	Move 10 meshes to temporary position	56.02
4	Return to main mesh stack	52.71
5	Move 10 meshes to temporary position	39.02
6	Move to designated area to change forklift lifting device	60.58
7	Change forklift lifting device	62.04
8	Move back to closest temporary mesh stack	24.27
9	Pick up mesh from stack	310.18
10	Move to formwork	402.34
11	Load mesh into formwork	302.68
12	Return to mesh stack	294.44
Total Time (seconds)		1738.17
Total Time (minutes)		28.97
Installation Time per Mesh Sheet (seconds)		57.94

Table 6
Activity chart for fabricating the mesh for an SG plank.

Task	Activity	Time (seconds)
1	Retrieve longitudinal reinforcement (7 bars)	28.18
2	Spread out longitudinal bars	6.56
3	Retrieve link bar (1 bar)	3.96
4	Install link bar at end of longitudinal bars	7.43
5	Walk to opposite end of longitudinal bars	4.86
6	Retrieve link bar (1 bar)	5.89
7	Install link bar at end of longitudinal bars	8.77
8	Retrieve link bar (1 bar)	2.91
9	Install link bar at end of longitudinal bars	4.96
10	Move 1 link bar to center of mesh	6.05
11	Retrieve transverse bars (28 bars)	17.17
12	Spread out transverse bars	28.34
13	Retrieve cable-tie tensioning device and ties	8.17
14	Fasten the GFRP bars together with cable ties (100 ties)	837.00
15	Retrieve additional cable ties	15.22
16	Place timber chocks on top of finished mesh (3 chocks)	11.62
Total Time (seconds)		997.09
Total Time (minutes)		16.62

Table 7
Activity chart for installing the mesh for an SG plank.

Task	Activity	Time (seconds)
1	Retrieve mesh from main mesh stack and walk to formwork	661.29
2	Walk over formwork	371.10
3	Place mesh into formwork	646.80
4	Return to main mesh stack	592.74
Total Time (seconds)		2271.93
Total Time (minutes)		37.87
Installation Time per Plank (seconds)		75.73

planks, thereby increasing the compression capacity of the uncracked concrete.

4.4. Deflection behavior

Fig. 12 shows the moment and mid-span displacement behavior of all the tested planks. They all exhibited a trilinear ascending response, which is consistent with the behavior reported in CSA-12 [44]. The first ascending response represents the uncracked concrete. Afterwards, a short second ascending behavior with a shallower linear slope than the first was observed, caused by the loss in stiffness when flexural cracks developed in the constant-moment zone. This observation is consistent with the results reported by El-Nemr, et al. [54]. The third ascending

Table 8
Activity chart for fabricating the mesh for a DG plank.

Task	Activity	Time (seconds)
1	Retrieve longitudinal reinforcement (5 bars)	27.48
2	Spread out longitudinal bars	3.97
3	Retrieve link bar (1 bar)	10.72
4	Install temporary link bar at end of longitudinal bars	11.83
5	Walk to opposite end of table	4.45
6	Retrieve link bar (1 bar)	4.96
7	Install temporary link bar at end of longitudinal bars	10.30
8	Retrieve link bar (1 bar)	6.24
9	Install temporary center link bar	8.83
10	Retrieve transverse bars (20 bars)	21.90
11	Spread out transverse bars	17.39
12	Retrieve cable-tie tensioning device and ties	17.66
13	Fasten the GFRP bars together with cable ties (76 ties)	515.00
14	Retrieve additional cable fixing ties	4.42
15	Place first layer onto the ground adjacent to work table	17.46
16	Retrieve longitudinal reinforcement (5 bars)	16.42
17	Spread out longitudinal bars	3.40
18	Install link bar at end of longitudinal bars	11.57
19	Walk to opposite end of table	4.63
20	Install link bar at end of longitudinal bars	10.12
21	Move link bar to center of mesh	4.99
22	Walk back to end of table	3.42
23	Retrieve link bar (1 bar)	4.92
24	Install link bar at end of longitudinal bars	6.97
25	Retrieve transverse bars (18 bars)	14.62
26	Spread out transverse bars	19.24
27	Retrieve cable-tie tensioning device and ties	14.57
28	Fasten the GFRP bars together with cable ties (70 ties)	554.00
29	Retrieve additional cable fixing ties	11.65
30	Retrieve first layer from ground	13.80
31	Install first layer onto existing link bars	16.23
32	Fasten the first and second mesh layers together with cable ties (6 ties)	73.32
Total Time (seconds)		1466.48
Total Time (minutes)		24.44

behavior is the cracking condition of the plank; the stiffness was governed by the type and layout of the reinforcement, and the concrete compressive strength. It should be mentioned that the second linear ascending behavior was very brief in the GS-reinforced concrete planks compared to the GFRP-reinforced ones which might be due to the higher stiffness of the galvanized steel bars compared to the GFRP bars which were able to retain higher stiffness after cracking. Due to the linear elastic behavior of the GFRP bars, the SG and DG planks exhibited a linear ascending response up to the maximum moment capacity (M_n), while the SS plank exhibited brief nonlinear behavior before the maximum M_n as the steel bars started to yield. After M_n , was reached, the moment and mid-span displacement curve experienced sudden drops due to concrete crushing either in the compression or shear zone. The 57% lower stiffness of plank SS-20–50 (3) compared to planks SS-20–50 (1) and SS-20–50 (2) could be due to the observed shear cracks, which reduced aggregate interlock and increased mid-span deflection. In contrast, the SG planks had almost similar behavior even with different reinforcement ratios and concrete compressive strength. This is inconsistent with the findings of Chang and Seo [13], who reported that the increase in reinforcement ratio increased the stiffness and prevented shear failure. This is also inconsistent with Theriault and Benmokrane [34] and Ashour [32], who indicated that increasing concrete strength increased the flexural capacity of the slabs. This might be due to the compression concrete layer being too thin, thereby reducing aggregate interlock, as was also observed by El-Sayed et al. [31]. Moreover, the dowel action was low when the reinforcement was at plank mid-depth as only the concrete above the longitudinal steel is resisting the shear. The DG planks had 25% greater flexural stiffness than the SG planks despite a lower reinforcement ratio (1/7th). Previous studies [33,58] suggested that increasing the reinforcement ratio significantly decreased the deflection. This finding cannot be

Table 9
Summary of mesh fabrication tasks, times, equipment, and labor.

	Mesh Fabrication			Mesh Installation		
	SS	SG	DG	SS	SG	DG
Number of operations	10	8	15	3	1	1
Number of transports	10	8	17	9	3	3
Number of delays	3	3	3	0	0	0
Total number of tasks	20	16	32	12	4	4
Total fabrication/installation time (minutes)	12.09	16.62	24.44	0.97	1.26	1.26
Mass of the reinforcing mesh (kg)	104.80	43.94	37.67	104.80	43.94	37.67
Number of workers required	2	2	2	6	4	4
Total worker minutes	24.18	33.24	48.88	5.82	5.04	5.04
Required equipment	Assembly table Hand drill Forklift	Assembly table Cable-tie tensioner	Assembly table Cable-tie tensioner	Forklift Crowbars to adjust position of installed mesh	No equipment required	No equipment required

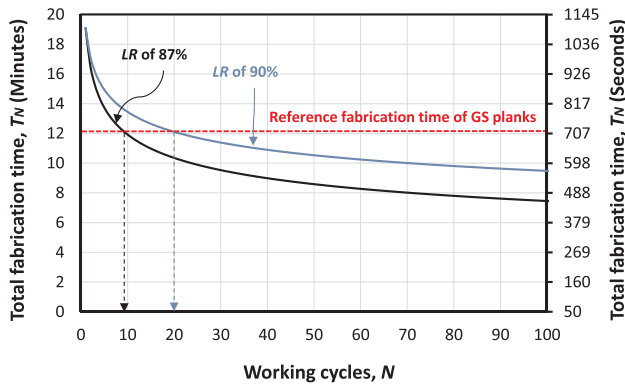


Fig. 8. Relationship of T_N time and work N cycles.

generalized unless the reinforcement in the planks is at the same effective depth. Once the effective depth increases, the shear-transfer mechanism will be enhanced as reported by Kim and Park [56] and El-Sayed et al. [31] due to aggregate interlock, reinforcement dowel action, and the depth of the uncracked concrete.

4.5. Flexural stiffness and toughness of planks

The flexural stiffness of a material can be denoted by its deformation curvature or the slope of the linear ascending line (the third ascending behavior as discussed in Fig. 12). Similarly, the flexural toughness or the ability to absorb energy can be represented by the area under moment-displacement curve, see Fig. 12. Table 12 reports the flexural stiffness (F_S) and toughness (F_T) values of the tested planks. The F_S and F_T values were normalized by dividing them to the gross area of

reinforcements (A_g). Clearly, GS-reinforced planks show more than three times higher F_S/A_g values compared to the singly GFRP-reinforced planks and SS planks. This increase is proportional to the difference in the elastic modulus between the two materials. However, increasing the effective depth of the GFRP reinforcements reduced the difference in F_S/A_g values. This is due to the concrete in the compressive zone adding resistance to the bending deformation. On the other hand, the GS-reinforced planks show better flexural toughness (F_T/A_g) than the singly GFRP-reinforced planks even with the lower curvature capacity. This is due to the lower moment capacity by the latter, where the behavior was governed by the shear failure as reported in Fig. 11 and Table 11. The higher F_T/A_g values of doubly GFRP-reinforced planks compared to SS planks is due to the lower slenderness ratio of the doubly GFRP-reinforced planks, which changed the failure from tension-shear to compression-shear leading to better stability and higher energy absorbing capacity prior failure. This can also be due to the linear elastic behavior of GFRP bars and high strain capacity to failure, which allows them to resist and deform more unlike the galvanized steel bars, which stop resisting additional bending moments after yielding.

4.6. Strength capacity of the reinforced-concrete planks

ACI-15 [59] recommends flexural-compression failure in concrete with GFRP-reinforced members because this type of failure is less brittle and has higher deformability compared to the tensile rupture of GFRP bars. To achieve this failure, ACI-15 [59] limits the ratio between the actual reinforcement ratio and the balanced reinforcement ratio (ρ_f/ρ_{bf}) to at least 1.4 [54]. In this study, the planks had a ρ_f/ρ_{bf} of around 1.51 (see Table 11). ρ_{bf} values were calculated in accordance with AS3600-2018 [2] for GS planks (see Eqns. A-(6–8)), while CSA-12 [44] was used for the GFRP planks (see Eqns. A-(3–5)), and tabulated in Table 11. Similarly, the shear-strength capacity of the concrete planks was

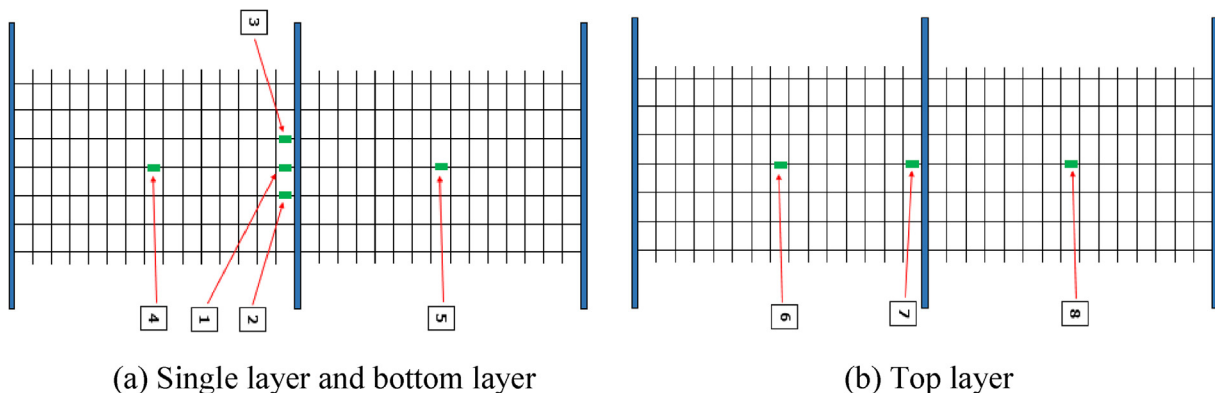


Fig. 9. Strain-gauge location.

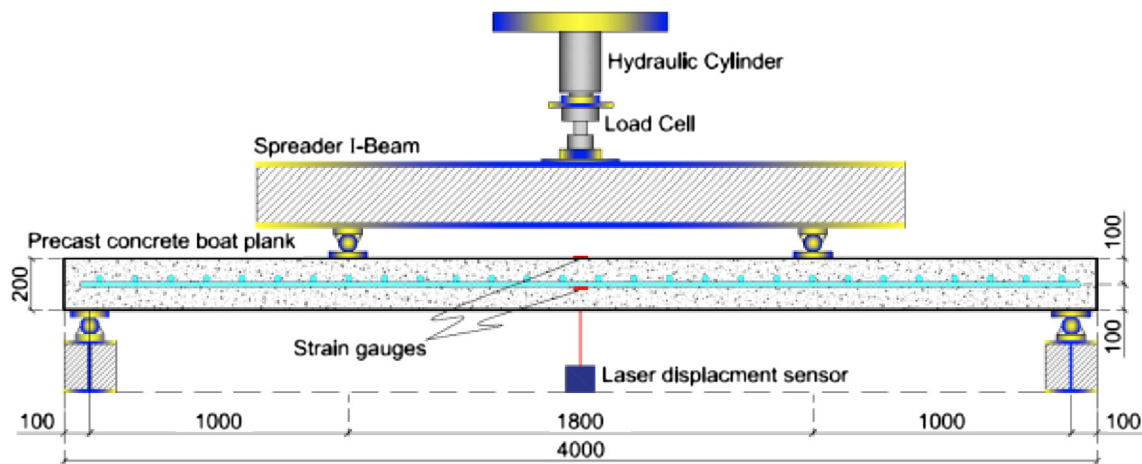


Fig. 10. Flexural test setup and instrumentation for the precast RC planks.

calculated. AS3600-2018 [2] was used to predict the flexural- and shear-strength capacities of the SS planks [Eqns. A-(9–11 and 19–20)], whereas CSAS806-12 [44] [Eqns. A-(12–14 and 21–23)] and ACI440.1R-15 [47] [Eqns. A-(15–18 and 24–26)] were adopted for the SG and DG planks. Table 13 shows that AS3600-2018 [2] showed very good prediction of the flexural capacity for the SS planks once including the self-weight, while a difference can be observed between the experimental and predicted values of the shear strength as the failure mode was flexural. On the other hand, CSAS806-12 [44] yielded better prediction of the shear strength for the SG planks when the self-weight of the planks is considered, compared to ACI440.1R-15 [47] as shown in Table 13. In contrast, both CSAS806-12 [44] and ACI440.1R-15 [47] underestimated the shear strength for the DG planks. Nevertheless, ACI440.1R-15 [47] significantly underestimated the shear strength capacity compared to the CSAS806-12 [44] design code which showed closer predicted results. The discrepancy between the predicted and actual shear strength could be due to the very high a/d ratio of the planks resulting from a thin concrete layer in compression specially after concrete cracking, low dowel action, and aggregate interlock, which is not considered in the ACI440.1R-15 [47] guidelines.

4.7. Strain behavior of the longitudinal bars

The ISIS design manual [61] and CSA-12 [44] suggest that not only the stress limit at the service load ($0.3M_n$) can be considered for serviceability purposes; the strain values in the longitudinal GFRP bars can also be used. The moment at a service load of 30% of M_n was considered, as suggested by Mota et al. [62], Kassem et al. [57], and El-Nemr et al. [54] for GFRP-reinforced one-way slabs and beams. The strain limit in the steel bars was derived from ACI 318–99 [63], which recommends adopting 60% of the yield strength (f_y), i.e., $1200 \mu\epsilon$ for steel with $f_y = 400$ MPa, which is the most common grade of steel reinforcement in Canada and the US. Moreover, by taking the ratio of 5/3 between the permissible crack width with GFRP bars (0.5 mm) and steel bars (0.3 mm), the new strain limit in GFRP bars for serviceability

($1200 \times 5/3$) is $2000 \mu\epsilon$. This arbitrary assumption cannot be directly adopted due to the different grades of steel used in Australia ($f_y = 500$ MPa). Interestingly, AS3600-2018 [2] recommends the same permissible crack width of $1200 \mu\epsilon$ for steel-reinforced beams and slabs. Correspondingly, the strain limit for GFRP bars should be $2500 \mu\epsilon$. Fig. 13 shows the strain values in the longitudinal reinforcement at mid-span against the applied moment. As expected, the galvanized steel exhibited bilinear strain behavior, as shown in Fig. 13a, while the GFRP reinforcement had trilinear strain behavior (Fig. 13b and 13c). The strain in the longitudinal reinforcement increased when the reinforcement ratio decreased, as was also observed in [23,54]. Therefore, SG-reinforced planks in Fig. 13b exhibited higher strain values with the increase of concrete strength and reinforcement ratio. These parameters, however, had little effect on the strain in double-layer planks with GFRP bars (Fig. 13c) due to the higher curvature as a result of the high mid-span displacement, thicker uncracked concrete resisting compression, and closer axial stiffness of the reinforcement, compared to the SS and SG planks.

4.8. Permissible crack width at serviceability limit state

The width of the first flexural crack observed in the plank was measured and plotted against the applied moment in Fig. 14. In Fig. 14a, planks SS-20–50 (1) and SS-20–50 (2) show almost identical cracking behavior up to $0.6M_n$, followed by reduced stiffness due to the development of major cracks at other plank locations. At $0.67M_n$, widening of the existing cracks was observed but not new cracks as noticed also by El-Nemr, Ahmed [54]. Fig. 14b shows a clear effect of higher concrete compressive strength and different axial stiffness of the reinforcement as plank SG-25–50 exhibited narrower cracks than plank SG-25–40. This could be due to increased aggregate interlock and the thick uncracked concrete layer resisting shear. Similarly, plank SG-25–40 shows narrower cracks compared to plank SG-20–40 due to the higher reinforcement ratio. These findings are consistent with the observations of El-Nemr, Ahmed [58]. On the other hand, planks DG-

Table 10
Theoretical and experimental cracking-moment values.

Sample	SS-20–50 (1)	SS-20–50 (2)	SS-20–50 (3)	SG-25–50	SG-25–40	SG-20–40	DG-13–50	DG-13–40	DG-16–40
f'_c (MPa)	52.1	52.1	52.1	52.1	40.7	40.7	52.1	40.7	40.7
Experimental P_{cr} (kN)	34.9	37.7	29.0	32.3	31.6	32.9	46.4	41.6	43.2
Experimental M_{cr} , excluding self-weight (kN.m)	17.5	18.9	14.5	16.2	15.8	16.5	23.2	20.8	21.6
Experimental M_{cr} , including self-weight (kN.m)	26.5	27.9	23.5	25.2	24.8	25.5	32.2	29.8	30.6
Theoretical $M_{cr,1}$ (kN.m)	27.4	27.4	27.4	27.4	24.2	24.2	27.4	24.2	24.2
Theoretical $M_{cr,2}$ (kN.m)	18.3	18.3	18.3	18.3	16.1	16.1	18.3	16.1	16.1

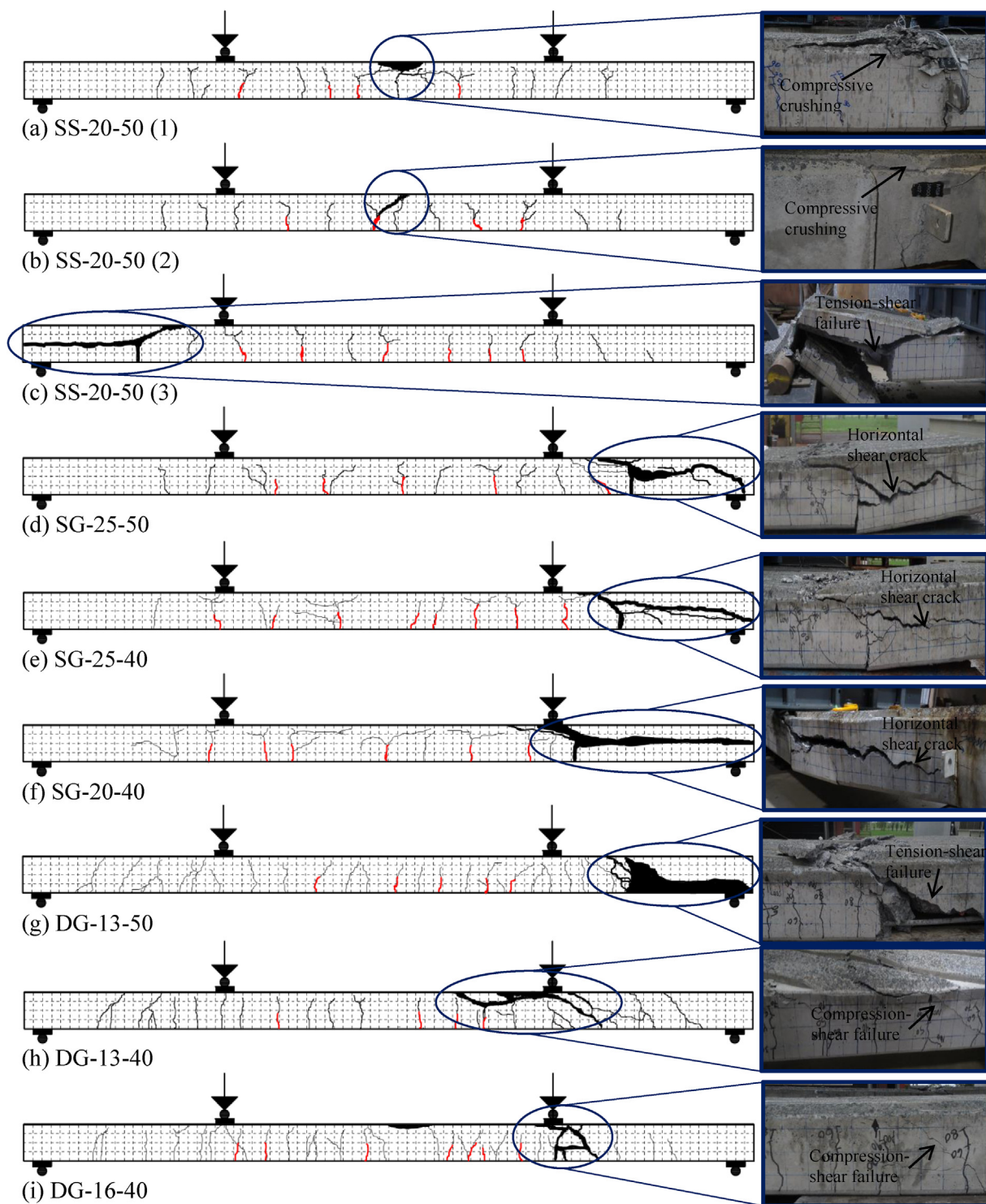


Fig. 11. Crack propagation and final failure of precast-concrete planks.

13–40 and DG-16–40 (see Fig. 14c) behaved similarly as they had the same concrete strength and almost equal amounts of longitudinal reinforcement. Plank DG-13–50 exhibited narrower cracks due to its higher concrete strength than planks DG-13–40 and DG-16–40.

It is important to note that CSA S806-12 [44] and ISIS Canada [45] recommend a maximum crack width of 0.5 mm for GFRP-reinforced concrete structures, while ACI-318-14 [54] recommends a maximum permissible crack width of 0.3 mm for steel-reinforced concrete structures exposed to exterior environments. Therefore, this study approached to investigate the relationship between the moment capacities

of the tested planks, corresponding to the maximum permissible crack width for both types of reinforced planks, to the strain of the reinforcing bars at that level of crack width. Thus, Fig. 14d summarizes the strain in the reinforcing bars to the service moment capacity ratio (M/M_u) at the permissible crack width. It should be highlighted that the service moment capacity ratio was considered as the ratio between the applied moment values correspond to the crack width limit divided by the theoretical moment strength (M_u) as suggested by AS3600-2018 [2] code for SS-reinforced planks and CSA S806-12 [44] for the GFRP-reinforced planks due to their close prediction of the experimental test

Table 11
Test results of the precast-concrete planks.

Specimen	ρ_{bf} (%)	ρ_f/ρ_{bf} (%)	a/d ratio	M_u (kN.m)	$\mu\epsilon_{max}$	δ_{max} (mm)	Failure Mode
SS-20-50 (1)	3.38	0.47	10.00	108.1	15,903	71.1	Compression
SS-20-50 (2)	3.38	0.47	10.00	111.5	15,924	69.5	Compression
SS-20-50 (3)	3.38	0.47	10.00	110.1	15,838	110.1	Tension-shear
SG-25-50	0.39	9.66	10.00	95.2	5938	112.4	Tension-shear
SG-25-40	0.31	11.96	10.00	89.5	6335	102.6	Tension-shear
SG-19-40	0.31	6.87	10.00	87.2	7599	105.5	Tension-shear
DG-13-50	0.38	1.51	6.25	135.7	15,873	134.2	Tension-shear
DG-13-40	0.31	1.87	6.25	132.3	15,594	135.5	Compression-shear
DG-16-40	0.32	2.01	6.25	139.0	15,772	128.7	Compression-shear

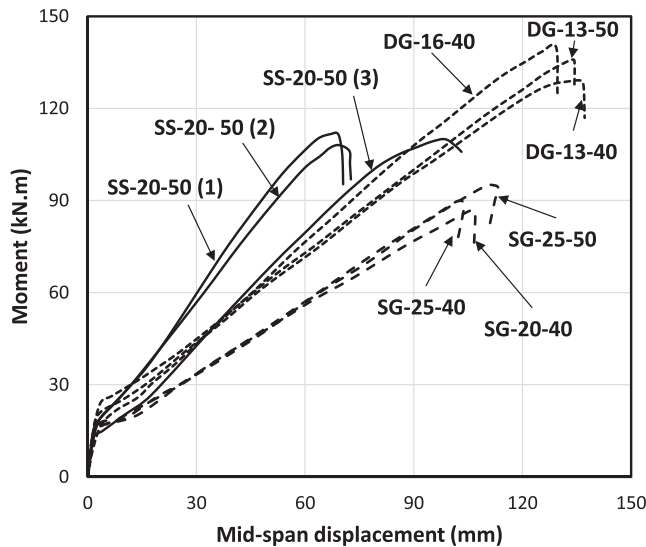


Fig. 12. Moment–displacement behavior of the tested planks.

results. Referring to the theoretical moment capacity was implemented due to the shear effect on the failure mode of tested planks. Regarding Fig. 14d, it can be noticed that SS-reinforced planks showed almost $1400 \mu\epsilon$ at the permissible crack width, which is very close to the strain limit of $1500 \mu\epsilon$ (60% of the yield strain ($2500 \mu\epsilon$)). Also, the service load at this level was just higher than 30% of M_u . In contrast, the suggested strain limit for the GFRP-reinforced flexural members by $2000 \mu\epsilon$ [44,45] was compared to the strain in the GFRP bars at the maximum permissible crack width. A clear divergent can be noticed between the strain values of the GFRP bars to the strain limit, which in some cases reached more than 400% (see Fig. 14d). Michaluk et al. [30], Chang and Seo [13], and El-Nemr et al. [54] reported that GFRP bars yielded high strain values at early loading stages compared to steel bars in flexural concrete members. This will result in a very conservative and inefficient design. At the same moment, all the GFRP-reinforced planks recorded more than 30% of M_u at the maximum

permissible crack width with very less conservativeness compared to the strain limit approach. Therefore, adopting $0.3M_u$ as a serviceability design limit results in more efficient design for the flexural GFRP-reinforced concrete planks than the strain design limit. This serviceability limit was also suggested by many researchers as the strain in GFRP bars can be affected by many factors, such as bar diameter, the number of bars, the nature and bond strength of the reinforcing bars [54,57,58], a/d ratio [13,64], and concrete compressive strength [34,58]. Moreover, it can be observed that all the GFRP-reinforced planks yielded higher cracking load capacity than the SS planks at the maximum permissible crack width. This indicates that GFRP bars are more effective than GS bars as reinforcement in precast-concrete boat-ramp planks.

4.9. Optimal boat-ramp planks reinforced with GFRP bars

The planks reinforced with two layers of GFRP bars (DG) performed significantly better than those with one layer (SS and SG planks). Despite having the lowest reinforcement ratio, the bending-moment capacity of the DG planks was 60% higher than the SG planks and 20% higher than the SS planks. In addition, the DG planks had the highest cracking moment because the bottom layers of GFRP reinforcement prevented the early development of flexural cracks. These planks were also the most effective in terms of the ratio of the maximum bending-moment capacity to the total area of longitudinal reinforcement, as shown in Table 14. While two layers of 12.7 mm bars (plank DG-13-40) were slightly better than two layers of 15.9 mm bars (plank DG-16-40), it is recommended to adopt the latter as it uses fewer bars and fewer cable ties in fastening the GFRP reinforcement together. Note that the comparative evaluation of manufacturing performance identified fastening the GFRP bars together with cable ties was the most time-consuming process in assembling plank reinforcement. The results also revealed no significant difference in the performance of GFRP-reinforced planks with 40 MPa and 50 MPa concrete. The capacity of the planks made with 50 MPa concrete (planks DG-13-50 and SG-25-50) was, at the most, only 6% higher than that of planks made with 40 MPa concrete (planks DG-13-40 and SG-25-40) due to the limited depth of the uncracked concrete. This result indicates that a compressive

Table 12
Stiffness and toughness of the tested specimens.

Specimen	$F_S (\frac{N \cdot mm}{mm} \times 10^3)$	$F_T (N \cdot mm^2 \times 10^6)$	$F_S/A_g (\frac{N \cdot mm}{mm^3})$	$F_T/A_g (\frac{N \cdot mm^2}{mm^2} \times 10^3)$
SS-20-50 (1)	1757	4665	799	2121
SS-20-50 (2)	1568	4714	713	2144
SS-20-50 (3)	1275	6825	580	3104
SG-25-50	796	6024	224	1699
SG-25-40	780	5328	220	1502
SG-19-40	756	5151	377	2568
DG-13-50	930	10,649	525	6010
DG-13-40	905	10,596	511	5980
DG-16-40	1042	10,436	525	5257

Table 13

Comparison between experimental and theoretical flexural and shear capacities.

Specimen	M_n^+ (kN.m)	M_n^{++} (kN.m)	V_n^+ (kN)	V_n^{++} (kN)	M_u (kN.m)	V_{uc} (kN)	M_u (kN.m)	V_{uc} (kN)
SS-20-50 (1)	108.1	117.1	108.1	117.1	126.7 *	161.7 *	–	–
SS-20-50 (2)	111.5	120.5	111.5	120.5	126.7 *	161.7 *	–	–
SS-20-50 (3)	110.1	119.1	110.1	119.1	126.7 *	161.7 *	–	–
SG-25-50	95.2	104.2	95.2	104.2	111.3 **	106.8 **	93.7***	40.4***
SG-25-40	89.5	98.5	89.5	98.5	98.0 **	98.3 **	84.1***	35.7***
SG-20-40	87.2	96.2	87.2	96.2	76.1 **	80.7 **	69.1***	27.2***
DG-13-50	135.7	144.7	135.7	144.7	126.6 **	82.8 **	119.5***	26.9***
DG-13-40	132.3	141.3	132.3	141.3	113.3 **	76.3 **	109.9***	23.8***
DG-16-40	139.0	148.0	139.0	148.0	116.6 **	78.5 **	112.5***	24.7***

* AS3600-2018 code + Excluding the self-weight.

** CSAS806-12 code ++ Including the self-weight.

*** ACI440.1R-15 guidelines.

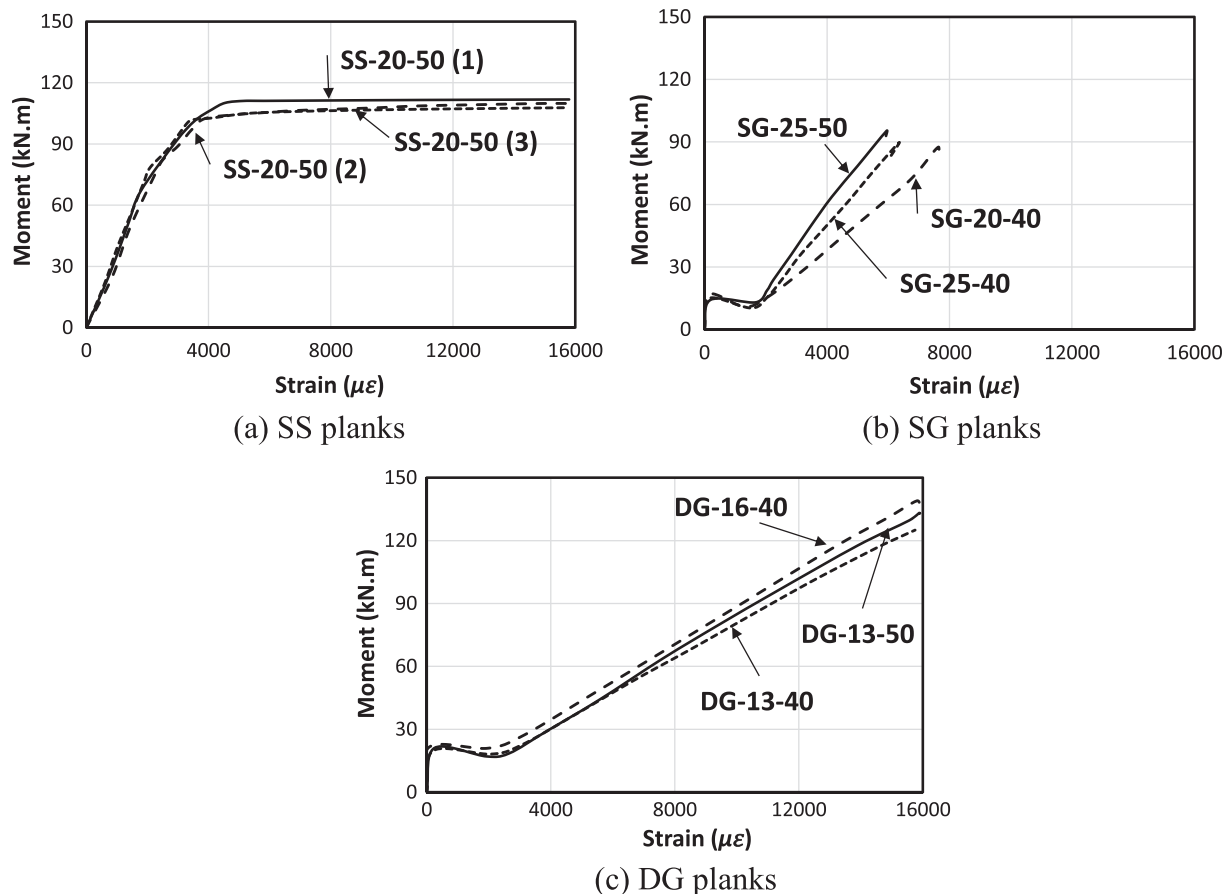
strength of 40 MPa is acceptable for precast boat-ramp planks reinforced with GFRP bars.

5. Installation of type rg4000 frp planks

Four (4) Type RG4000 FRP planks were installed as part of the lengthening and partial reconstruction of the Parkyn Parade upstream boat ramp in Mooloolaba, Sunshine Coast, Australia (Fig. 15). The entire installation process was monitored, documented, and compared to the installation procedure for GS-reinforced precast-concrete boat-ramp planks (Type RG4000). No differences in the installation process were observed between the galvanized-steel-reinforced boat-ramp planks and the GFRP-reinforced planks in terms of tasks, time, equipment, and labor. Therefore, the different designs have no financial impact due to new installation procedures. The required activities—including

preparing the bed for the planks with crushed rock and geogrid; lifting, moving, laying, and levelling the planks; and locking the planks together with stainless-steel bolts, nuts, and washers—are the same. The main observations during installation are provided below.

- Full installation of the Type RG4000 FRP planks required the same number of workers and equipment as Type RG4000 planks.
- The Type RG4000 FRP planks required the same total number of tasks for complete installation as Type RG4000 planks due to similar design and better structural performance.
- The total installation time for the Type RG4000 FRP planks was the same as for Type RG4000 planks, since no extra processes were needed.
- The GFRP bars did not entail additional installation costs related to weight or extra workload.

**Fig. 13.** Moment and longitudinal-bar strain in precast boat-ramp planks.

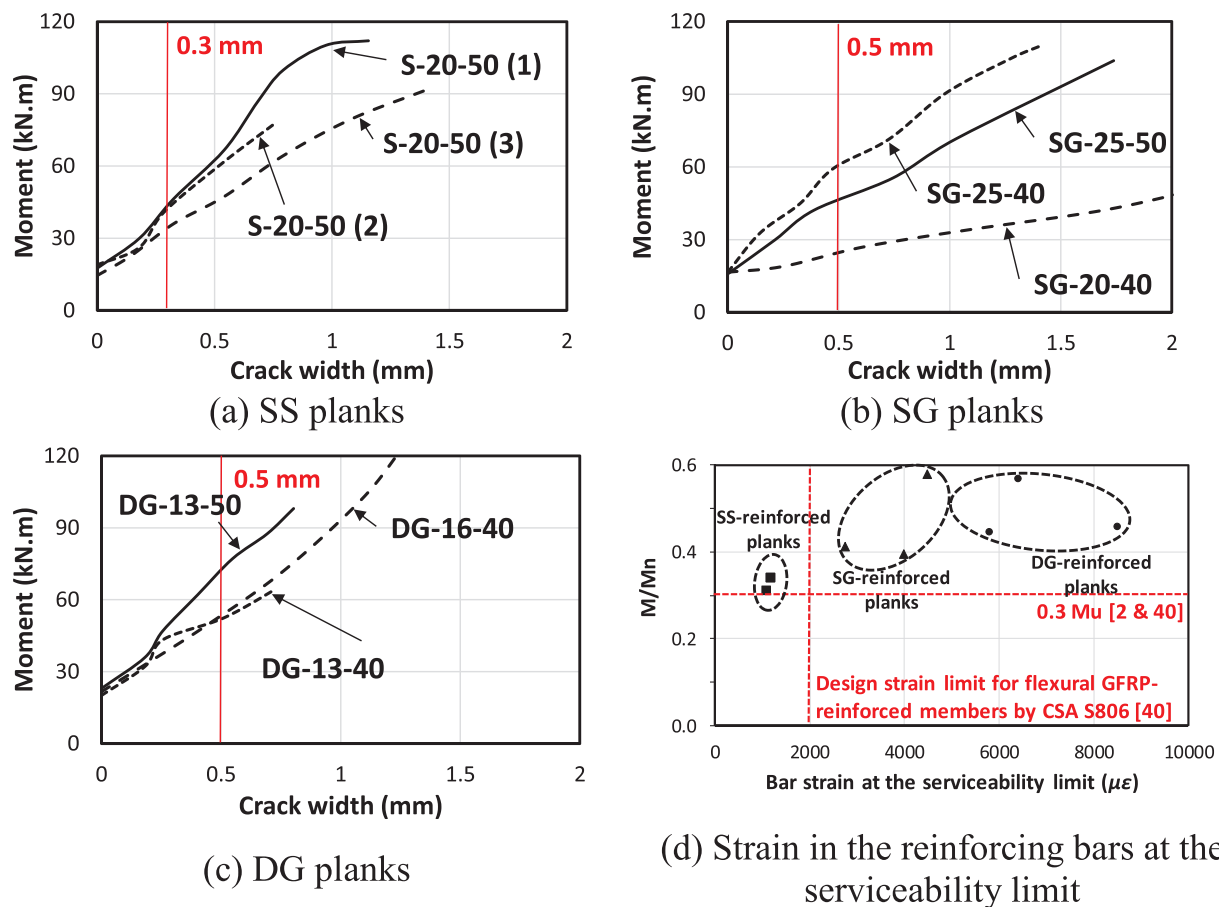


Fig. 14. Relationship of moment and crack width.

Table 14
Evaluation of plank effectiveness.

Plank	M_n (kNm)	Total Bar Area, A_g (mm ²)	M_n/A_g (N-m/mm ²)
SS-1-20-50 (1)	112	2199	50.93
SS-1-20-50 (2)	108	2199	49.11
SS-20-50 (3)	110	2199	50.02
SG-25-50	96	3546	26.93
SG-25-40	90	3546	25.38
SG-20-40	81	2006	40.37
DG-13-50	136	1772	76.75
DG-13-40	129	1772	72.80
DG-16-40	140	1985	70.52

In addition, the lighter weight of Type RG4000 FRP planks of around 70 kg per plank (GFRP reinforcing mesh instead of galvanized-steel mesh) might result in less workload during handling, lifting, and even in transportation and delivery.

6. Conclusions

This comparative study evaluated the manufacturing and structural performance of precast-concrete boat-ramp planks reinforced with GFRP bars and planks conventionally reinforced with galvanized-steel bars. It focused on the effective design, trial manufacture, time-and-motion study of the manufacturing process, investigation of the structural performance, and installation of planks in an actual boat-ramp project, leading to the development of industry-accepted GFRP-reinforced boat-ramp planks. From the test results and analysis of this study, the following conclusions can be drawn:

- The fabrication of precast-concrete boat-ramp planks with GFRP bars involved less labor and equipment, and the planks will have better structural performance than galvanized-steel-reinforced planks. Due to the non-corroding properties of composite reinforcing bars, the use of expensive silica fume—added to make concrete watertight and minimize the corrosion of steel in marine environments—can be eliminated.
- The fabrication and installation of the reinforcing mesh are the main processes different between GFRP-reinforced (SG and DG planks) and galvanized-steel-reinforced (SS) planks. The SS planks had the fastest mesh fabrication time, requiring only 24.18 worker-minutes, followed by the SG planks (33.24 worker-minutes). The DG planks had the slowest fabrication time (48.88 worker-minutes) because the process required a total of 32 tasks, 17 of which related to material handling.
- Tying the reinforcement together was the process requiring the longest time. This task constituted up to 60% and 70% of the total fabrication process of the meshes reinforced with galvanized steel and GFRP, respectively.
- Installing the GFRP reinforcing mesh into the formwork was 13% faster than installing the galvanized-steel reinforcing mesh. Moreover, two workers were able to carry the GFRP reinforcing mesh manually while the galvanized-steel reinforcing mesh required a forklift in handling, transportation, and storage.
- The learning-curve model using a 90% learning rate showed that, after 20 work cycles, the mesh fabrication time for GFRP bars could equal or possibly be less than that of the standard single-layer mesh made with galvanized steel. With ongoing task repetition and training, the overall process will become efficient, further reducing the time taken by workers to complete tasks.
- The increased effective depth with a double-layer of GFRP bars

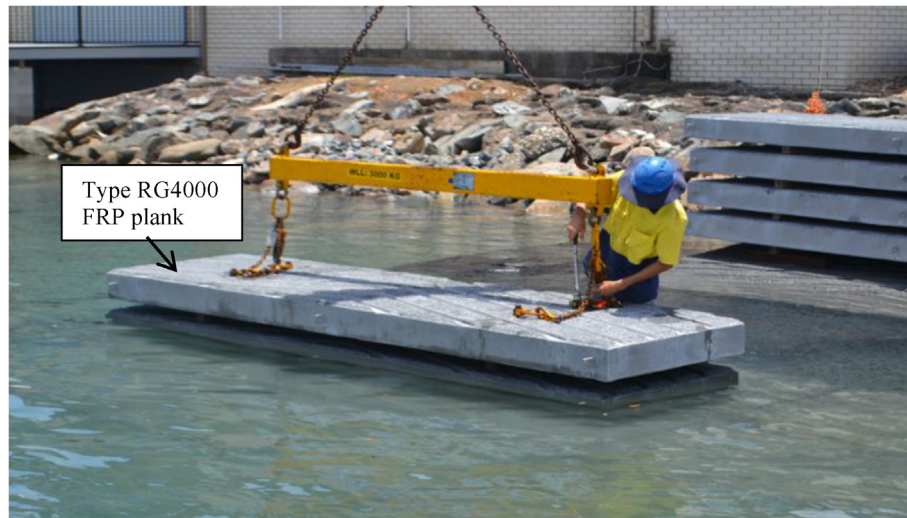


Fig. 15. Installation of Type RG4000 FRP planks.

yielded a cracking moment at least 10% higher than with galvanized-steel reinforcement due to the bottom bars acting as links for better continuity within the concrete section. It also narrowed the crack widths and prevented failed concrete from falling off the planks.

- The precast-concrete boat-ramp planks reinforced with two layers of GFRP bars exhibited significantly higher structural performance than the planks with one layer of galvanized-steel or GFRP bars. Even though they had the lowest reinforcement ratio, these planks had a bending-moment capacity 60% higher than the planks with a single layer of GFRP bars and 20% higher than the planks reinforced with galvanized steel due to the bottom bars assisting in resisting the widening of cracks on the bottom of the planks. Moreover, the flexural stiffness and toughness of these planks are at least twice that planks reinforced with single layers of GFRP bars and galvanized steel bars.
- The capacity of the planks made with 50 MPa concrete was at most 6% higher than that of the planks made with 40 MPa concrete due to the limited depth of the uncracked concrete. This suggests that a compressive strength of 40 MPa is acceptable for precast-concrete boat-ramp planks reinforced with GFRP bars.
- Two layers of 15.9 mm GFRP bars was found to be optimum as it involves fewer bars and cable ties to fasten the GFRP reinforcement together. This design also resulted in the most effective usage of the high tensile strength of the GFRP bars. At failure, the strain in the longitudinal bars was around 15,000 $\mu\epsilon$ or 70% of the ultimate failure tensile strain, while the measured strain for single layer of bars was 5,000 $\mu\epsilon$, which is only 23% of the ultimate failure strain of the GFRP bars.
- There was no difference in the installation process with the galvanized-steel-reinforced planks and the GFRP-reinforced planks in terms of tasks, time, equipment, and labor required. The lower weight of the Type RG4000 FRP planks, however, reduced the workload during handling, lifting, and even in transportation and delivery.

New opportunities for documenting and directly comparing the fabrication process between batches of GFRP- and galvanized-steel-reinforced planks would further confirm that Type RG4000 FRP planks could be fabricated at a cost comparable to planks made with galvanized steel while yielding enhanced durability. Moreover, specifying the use of Type RG4000 FRP planks in future marine infrastructure projects would further demonstrate the technology's many benefits and lead to its widespread use.

Declaration of Competing Interest

The authors declare that they have no known competing financial interests or personal relationships that could have appeared to influence the work reported in this paper.

Acknowledgements

The authors would like to thank the Queensland Department of Transport and Main Roads (DTMR) and the Advance Queensland Industry Research Fellowship Program (AQIRF 119-2019RD2) for the financial support. The authors also acknowledge the Natural Science and Engineering Research Council (NSERC) of Canada, and GFRP Reinforcing Pty Ltd for providing the GFRP reinforcements. The authors are grateful to SkillCentred Pty Ltd for fabricating the precast-concrete boat-ramp planks and for the assistance from technicians and students at the University of Southern Queensland during plank manufacturing and testing.

Appendix

This section includes the design equations used in this study.

- Cracking-moment equations:

$$M_{cr} = \left(\frac{f_r}{y_t} \right) I_g \quad \text{A-(1)}$$

$$f_{r,1} = 0.6 \sqrt{f'_c} \quad [44,45] \quad \text{A-2(a)}$$

$$f_{r,2} = 0.4 \sqrt{f'_c} \quad [53] \quad \text{A-2(b)}$$

- Balanced reinforcement-ratio equations:

$$\rho_{bf} = \alpha_1 \beta_1 \frac{f'_c}{f_{fu}} \frac{E_f(0.0035)}{E_f(0.0035) + f_{fu}} \quad [44] \quad \text{A-(3)}$$

$$\alpha_1 = 0.85 - 0.0015 f'_c; 0.85 \geq \alpha_1 \geq 0.67 \quad [44] \quad \text{A-(4)}$$

$$\beta_1 = 0.97 - 0.0025 f'_c; 0.97 \geq \beta_1 \geq 0.67 \quad [44] \quad \text{A-(5)}$$

$$\rho_{bst} = \frac{\alpha_2 f'_c \gamma \left(\frac{(0.003)d}{0.0025 + 0.003} \right) b}{f_{sy}(bd)} \quad [2] \quad \text{A-(6)}$$

$$\alpha_2 = 1.00 - 0.003 f'_c; 0.85 \geq \alpha_2 \geq 0.67 \quad [2] \quad \text{A-(7)}$$

$$\gamma = 1.05 - 0.007 f'_c; 0.85 \geq \gamma \geq 0.67 \quad [2] \quad \text{A-(8)}$$

- Flexural-strength capacity:

$$M_u = A_{st} f_s \left(d - \frac{\gamma d_n}{2} \right) \quad [2] \text{ A-(9)}$$

$$d_n = \frac{-1 \pm \sqrt{1^2 - 4 \left(\frac{\alpha_2 f_c \gamma b}{0.003 A_{st} E_s} \right) (-d)}}{2 \left(\frac{\alpha_2 f_c \gamma b}{0.003 A_{st} E_s} \right)} \quad [2] \text{ A-(10)}$$

$$f_s = \frac{\alpha_2 f_c \gamma d_n b}{A_{st}} \quad [2] \text{ A-(11)}$$

$$M_u = A_{st} f_f \left(d - \frac{\beta_1 d_n}{2} \right) \quad [44] \text{ A-(12)}$$

$$d_n = \frac{-1 \pm \sqrt{1^2 - 4 \left(\frac{\alpha_1 f_c \beta_1 b}{0.003 A_{st} E_f} \right) (-d)}}{2 \left(\frac{\alpha_1 f_c \beta_1 b}{0.003 A_{st} E_f} \right)} \quad [44] \text{ A-(13)}$$

$$f_{GFRP} = \frac{\alpha_1 f_c \beta_1 d_n b}{A_{st}} \quad [44] \text{ A-(14)}$$

$$\beta_1 = 0.85 - \frac{0.05(f_c' - 27.6)}{6.9} \quad [47] \text{ A-(15)}$$

$$\alpha_1 = 0.85 \quad [47] \text{ A-(16)}$$

$$M_n = \rho_f f_f \left(1 - 0.59 \frac{\rho_f f_f}{f_c} \right) b d^2 \quad [47] \text{ A-(17)}$$

$$f_f = \sqrt{\frac{(E_f \varepsilon_{cu})^2}{4} + \frac{0.85 \beta_1 f_c E_f \varepsilon_{cu}}{\rho_f} - 0.5 E_f \varepsilon_{cu}} \leq f_{fu} \quad [47] \text{ A-(18)}$$

- Shear-strength capacity equations:

$$V_{uc} = \beta_{1*} \beta_2 \beta_3 b d f_{cv} \left(\frac{A_{st}}{b d} \right)^{1/3} \quad [2] \text{ A-(19)}$$

$$\beta_{1*} = 1.1 (1.6 - d/1000) \geq 0.8 \quad [2] \text{ A-(20)}$$

$$V_{uc} = 0.05 \lambda k_m k_r (f_c')^{1/3} b d_v \quad [44] \text{ A-(21)}$$

$$k_m = \sqrt{\frac{V_f d}{M_f}} \leq 1.0 \quad [44] \text{ A-(22)}$$

$$k_r = 1 + (E_f \rho_f)^{1/3} \quad [44] \text{ A-(23)}$$

$$V_{uc} = \frac{2}{5} \sqrt{f_c'} b c \quad [47] \text{ A-(24)}$$

$$c = k d \quad [47] \text{ A-(25)}$$

$$k = \sqrt{2 \rho_f n_f - (\rho_f n_f)^2} - \rho_f n_f \quad [47] \text{ A-(26)}$$

References

- [1] DTMR, Design Criteria for Boat Ramps. Queensland Department of Transport and Main Roads, Brisbane, Queensland, 2015.
- [2] Australian Standards AS3600:2018, Concrete Structures. Standards Australia Limited, Sydney, New South Wales 2001, Australia.
- [3] DTMR-2016a, Structures Inspection Manual Part 2: Deterioration Mechanisms. Queensland Department of Transport and Main Roads, Brisbane, Queensland, 2016.
- [4] Mehta PK. Durability-critical issues for the future. *Concr Int* 1997;19(7):27–33.
- [5] Shayan, A. and A. Xu, Realising 100-year bridge design life in an aggressive environment: review of the literature. 2016.
- [6] Queensland, M.S., Waterways: Recreational boating infrastructure. Queensland Department of Transport and Main Roads, Brisbane, Queensland, 2018.
- [7] Cassidy, M., J. Waldie, and S. Palanisamy, A Method to Estimate the Cost of Corrosion for Australian Defence Force Aircraft. 2015.
- [8] Yalciner H, Eren O, Sensoy S. An experimental study on the bond strength between reinforcement bars and concrete as a function of concrete cover, strength and corrosion level. *Cem Concr Res* 2012;42(5):643–55.
- [9] Mehta PK. Advancements in concrete technology. *Concr Int* 1999;21(6):69–76.
- [10] Cabral A, et al. The corrosion resistance of hot dip galvanised steel and AA2024-T3 pre-treated with bis-[triethoxysilylpropyl] tetrasulfide solutions doped with Ce (NO₃)₃. *Corros Sci* 2006;48(11):3740–58.
- [11] Nkurunziza G, et al. Durability of GFRP bars: a critical review of the literature. *Prog Struct Mat Eng* 2005;7(4):194–209.
- [12] Hardwicke L. Australian infrastructure report card. Barton, ACT: Engineers Australia; 2005.
- [13] Chang K, Seo D. Behavior of one-way concrete slabs reinforced with GFRP bars. *J Asian Archit Build Eng* 2012;11(2):351–8.
- [14] Patel VI, et al. Numerical analysis of circular double-skin concrete-filled stainless steel tubular short columns under axial loading. *Structures* 2020;24:754–65.
- [15] Dong M, Lokuge W, Elchalakani M, Karrech A. Modelling glass fibre-reinforced polymer reinforced geopolymer concrete columns. *Structures* 2019;20:813–21.
- [16] Manalo A, et al. Recent developments on FRP bars as internal reinforcement in concrete structures. *Concr Australia* 2014;40(2):46–56.
- [17] Benmokrane B, et al. Field durability study of vinyl-ester-based GFRP rebars in concrete bridge barriers. *J Bridge Eng* 2018;23(12):04018094.
- [18] Benmokrane B, et al. Laboratory assessment and durability performance of vinyl-ester, polyester, and epoxy glass-FRP bars for concrete structures. *Compos B Eng* 2017;114:163–74.
- [19] Benmokrane B, et al. Effects of diameter on the durability of glass fiber-reinforced polymer bars conditioned in alkaline solution. *J Compos Constr* 2017;21(5):04017040.
- [20] Manalo A, et al. Comparative durability of GFRP composite reinforcing bars in concrete and in simulated concrete environments. *Cem Concr Compos* 2020;103:564.
- [21] Kazemi M, et al. Non-linear behaviour of concrete beams reinforced with GFRP and CFRP bars grouted in sleeves. *Structures* 2020;23:87–102.
- [22] Al-Rubaye M, et al. Flexural behaviour of concrete slabs reinforced with GFRP bars and hollow composite reinforcing systems. *Compos Struct* 2019;118:836.
- [23] Jumaa GB, Yousif AR. Numerical modeling of size effect in shear strength of FRP-reinforced concrete beams. *Structures* 2019;20:237–54.
- [24] Maranan G, et al. Shear behavior of geopolymer concrete beams reinforced with glass fiber-reinforced polymer bars. *ACI Struct J* 2017;114(2).
- [25] Hasan HA, et al. Maximum axial load carrying capacity of Fibre Reinforced-Polymer (FRP) bar reinforced concrete columns under axial compression. *Structures* 2019;19:227–33.
- [26] AlAjarmeh OS, et al. Axial performance of hollow concrete columns reinforced with GFRP composite bars with different reinforcement ratios. *Compos Struct* 2019;213(1):12.
- [27] AlAjarmeh OS, et al. Compressive behavior of axially loaded circular hollow concrete columns reinforced with GFRP bars and spirals. *Constr Build Mater* 2019;194:12–23.
- [28] AlAjarmeh OS, et al. Novel testing and characterization of GFRP bars in compression. *Constr Build Mater* 2019;Volume 25. pp. 1112–1126.
- [29] AlAjarmeh OS, et al. Effect of spiral spacing and concrete strength on behavior of GFRP-reinforced hollow concrete columns. *J Compos Constr* 2019;24(1):04019054.
- [30] Michalak CR, et al. Flexural behavior of one-way concrete slabs reinforced by fiber reinforced plastic reinforcements. *ACI Struct J* 1998;95:353–65.
- [31] El-Sayed A, El-Salakawy E, Benmokrane B. Shear strength of one-way concrete slabs reinforced with fiber-reinforced polymer composite bars. *J Compos Constr* 2005;9(2):147–57.
- [32] Ashour SA. Effect of compressive strength and tensile reinforcement ratio on flexural behavior of high-strength concrete beams. *Eng Struct* 2000;22(5):413–23.
- [33] Mousavi SR, Esfahani MR. Effective moment of inertia prediction of FRP-reinforced concrete beams based on experimental results. *J Compos Constr* 2012;16(5):490–8.
- [34] Theriault M, Benmokrane B. Effects of FRP reinforcement ratio and concrete strength on flexural behavior of concrete beams. *J Compos Constr* 1998;2(1):7–16.
- [35] Nystrom HE, et al. Financial viability of fiber-reinforced polymer (FRP) bridges. *J Manage Eng* 2003;19(1):2–8.
- [36] Berg AC, et al. Construction and cost analysis of an FRP reinforced concrete bridge deck. *Constr Build Mater* 2006;20(8):515–26.
- [37] Achillides Z, Pilakoutas K. Bond behavior of fiber reinforced polymer bars under direct pullout conditions. *J Compos Constr* 2004;8(2):173–81.
- [38] Standard, A., AS5100. 2-2004, Bridge design—Part 2: design loads. Standards Australia, Sydney (Australia), 2004.
- [39] DTMR-2017a, Transport and Main Roads Specifications-MRTS72 Manufacture of Precast Concrete Elements. Queensland Department of Transport and Main Roads, Brisbane, Queensland, 2017.
- [40] DTMR-2017b, Transport and Main Roads Specifications MRTS70 Concrete. Queensland Department of Transport and Main Roads, Brisbane, Queensland, 2017.
- [41] DTMR-2017c, Transport and Main Roads Specifications MRTS300 Boat Ramps. Queensland Department of Transport and Main Roads, Brisbane, Queensland, 2017.
- [42] Australia, S. and S.N. Zealand, AS/NZS 4671: 2001 Steel reinforcing materials. 2001, Standards Australia International Ltd and Standards New Zealand Sydney.
- [43] DTMR-2016b, SD4000 - Precast planks for boat ramp - Types RG4000 and RG3500. Queensland Department of Transport and Main Roads, Brisbane, Queensland, 2016.
- [44] CSA, Design and construction of building structures with fibre-reinforced polymers. Canadian Standards Association, CAN/CSA-S806-12 2012 Rexdale ON, Canada.
- [45] 3, I.D.M.N., Reinforced concrete structures with fibre-reinforced polymers. ISIS Canada Research Network. Winnipeg, MB: University of Manitoba, 2007: p. 151.
- [46] SkillCentred, <http://www.skillcentred.com/skillcentred-constructions/>. 2018.
- [47] ACI, Guide for the Design and Construction of Concrete Reinforced with FRP Bars (440.1R-15). American Concrete Institute, Farmington Hills, MI, 2015.
- [48] DTMR-2018, SD4003 - Precast planks for boat ramp - Type RG4000 FRP. Queensland Department of Transport and Main Roads, Brisbane, Queensland, 2018.
- [49] Van Den Einde L, Zhao L, Seible F. Use of FRP composites in civil structural applications. *Constr Build Mater* 2003;17(6–7):389–403.
- [50] Meyers, F. and J. Stewart, Motion and Time Study for Lean Manufacturing. 3rd edn Pearson Education 2002 Upper Saddle River New Jersey, USA.
- [51] Jaber, M.Y., Learning curves: Theory, models, and applications. 2016: CRC Press.
- [52] Groover, M.P., Automation, production systems, and computer-integrated manufacturing. 2007: Prentice Hall Press.
- [53] CSA, Canadian highway bridge design code. Rexdale, ON, Canada: CAN/CSA S6-14. 2014: p. 733.
- [54] El-Nemr A, et al. Evaluation of the flexural strength and serviceability of concrete beams reinforced with different types of GFRP bars. *Eng Struct* 2018;173:606–19.
- [55] Kani G. Basic facts concerning shear failure. *J Proc* 1966.
- [56] Kim J-K, Park Y-D. Prediction of shear strength of reinforced concrete beams without web reinforcement. American Concrete Institute; 1996.
- [57] Kassem C, Farhaly AS, Benmokrane B. Evaluation of flexural behavior and serviceability performance of concrete beams reinforced with FRP bars. *J Compos Constr* 2011;15(5):682–95.
- [58] El-Nemr A, Ahmed EA, Benmokrane B. Flexural behavior and serviceability of normal-and high-strength concrete beams reinforced with glass fiber-reinforced polymer bars. *ACI Struct J* 2013;110(6).
- [59] 440, A.C., Guide for the design and construction of concrete reinforced with FRP bars (ACI 440.1R-15). Farmington Hills, MI: American Concrete Institute, 2015:

- p. 85.
- [61] No.3, I.D.M., Reinforcing Concrete Structures with Fibre Reinforced Polymers. Intelligent Sensing for Innovative Structures Canada, Winnipeg, 2001.
 - [62] Mota C, Alminar S, Svecova D. Critical review of deflection formulas for FRP-RC members. *J Compos Constr* 2006;10(3):183–94.
 - [63] ACI 318-99, Building Code Requirements for Structural Concrete. American Concrete Institute, Farmington Hills, Michigan, 1999.
 - [64] Alam M, Hussein A. Effect of member depth on shear strength of high-strength fiber-reinforced polymer-reinforced concrete beams. *J Compos Constr* 2012;16(2):119–26.